

1 **Divergence in climate model projections of future Arctic Ocean stratification**
2 **and hydrography**

3 Morven Muilwijk,^{a,b} Aleksi Nummelin,^c Lars H. Smedsrud,^b Igor V. Polyakov,^d Hannah
4 Zanowski,^e and Céline Heuzé,^f

5 ^a *Norwegian Polar Institute, Tromsø, Norway*

6 ^b *Geophysical Institute, University of Bergen and Bjerknes Centre for Climate Research, Bergen,*
7 *Norway*

8 ^c *Norwegian Research Centre and Bjerknes Centre for Climate Research, Bergen, Norway*

9 ^d *International Arctic Research Center and College of Natural Sciences and Mathematics,*
10 *University of Alaska Fairbanks, Fairbanks, US*

11 ^e *Department of Atmospheric and Oceanic Sciences, University of Wisconsin-Madison, Madison,*
12 *US*

13 ^f *Department of Earth Sciences, University of Gothenburg, Gothenburg, Sweden*

This manuscript has been submitted for publication in Journal of Climate and is currently undergoing peer-review.

Subsequent versions of this manuscript may have different content.

If accepted, the final version of this manuscript will be available via the "Peer-reviewed publication DOI" link on the right-hand side of this page and will be available under open-access on the publisher's website.

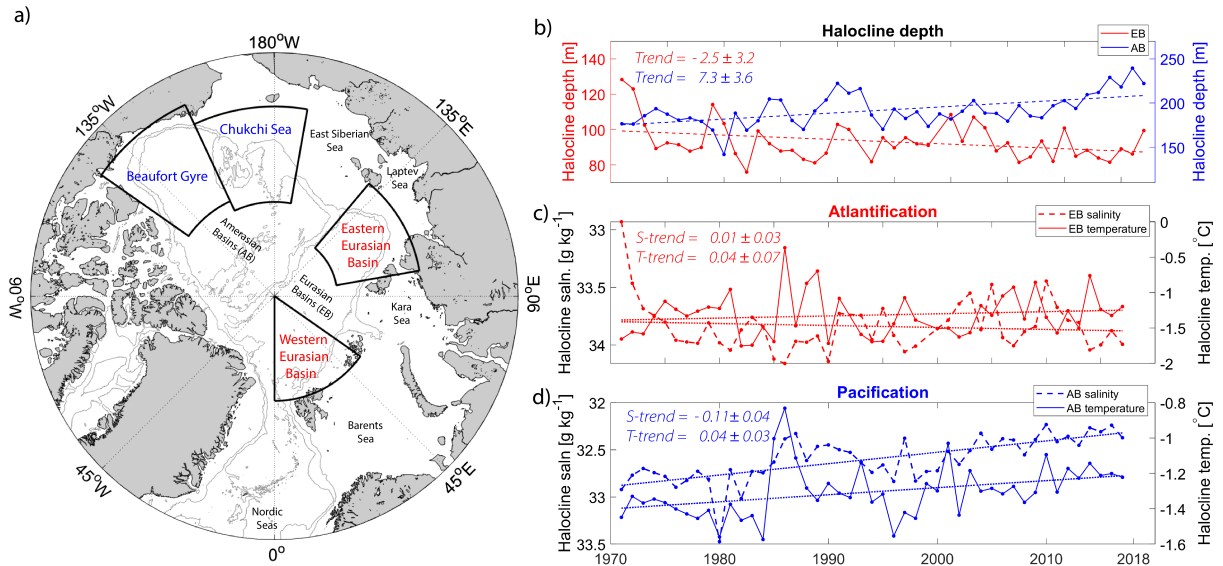
For any questions, contact the lead author Morven Muilwijk

15 ABSTRACT: The Arctic Ocean is strongly stratified by salinity gradients in the uppermost layers.
16 This stratification is a key attribute of the region as it acts as an effective barrier for the vertical
17 exchanges of Atlantic Water heat, nutrients, and CO₂ between intermediate depths and the surface
18 of the Eurasian and Amerasian basins (EB and AB). Observations show that from 1970 to 2017,
19 the stratification in the AB has strengthened, whereas, in parts of the EB, the stratification has
20 weakened. The strengthening in the AB is linked to a freshening and deepening of the halocline.
21 In the EB, the weakened stratification is linked to advection of saltier halocline waters and is
22 associated with a shoaling of the halocline (Atlantification). Future simulations from a suite of
23 CMIP6 models project that, under a strong greenhouse-gas forcing scenario (ssp585), the overall
24 surface freshening and warming in both basins continue, but there is a spread in hydrographic
25 trends across the models with even opposite trends in certain regions. Within the AB, there is
26 agreement among the models that the upper layers will become more stratified. However, within
27 the EB models diverge regarding future stratification. The divergence is due to different balances
28 between trends in the upper ocean, related to surface freshwater input, and trends at depth, related
29 to fluxes through Fram Strait. From these simulations, one could conclude that Atlantification will
30 not spread eastward into the AB; however, we need to improve models to simulate tendencies in a
31 more delicately stratified EB correctly.

32 **1. Introduction**

33 Much of the present-day central Arctic Ocean is a so-called beta ocean - it is strongly stratified by
34 salinity, unlike subtropical seas where the upper layers are permanently stratified by temperature
35 (Nansen 1902; Carmack 2007). Over the last few decades, the Arctic region has experienced
36 surface warming at more than twice the global rate (Cohen et al. 2020; IPCC 2021), and an
37 intensive loss of Arctic sea ice and glacial ice (Stroeve and Notz 2018; Shepherd et al. 2020).
38 These changes are associated with increased freshwater fluxes into the upper ocean (Solomon
39 et al. 2021, and references therein), and changes in the intermediate and deeper layers (Årthun and
40 Eldevik 2016). Even if the increasing trend in freshwater input to the Arctic Ocean is projected
41 to continue (Zanowski et al. 2021), a stronger subpolar influence (borealization; Polyakov et al.
42 2020a) and the simultaneous loss of sea ice (Notz and SIMIP~Community 2020) make the expected
43 stratification changes non-trivial. For the first time, we aim to provide an overview of the changing
44 Arctic stratification using unique historical observations and future model projections.

45 Typically, the upper part of the water column in the deep Arctic basins (Eurasian basin and
46 Amerasian basin, EB, and AB) is characterized by two distinct layers: a fresh and cold surface
47 layer and a warmer and saline layer at depth with water of Atlantic origin (Rudels 2015). There is
48 a cold halocline between them where the salinity increases rapidly with depth. This stratification
49 is one of the essential attributes of the Arctic Ocean, acting as an effective barrier for water mass
50 mixing and hence vertical exchanges (Peralta-Ferriz and Woodgate 2015). The strong layering
51 effectively shields the sea ice cover from oceanic heat found at depth (Nansen 1902; Aagaard
52 et al. 1981), limits primary production due to reduced nutrient fluxes (Randelhoff et al. 2020), and
53 reduces the ocean's capability to take up atmospheric CO₂ (Yasunaka et al. 2018). The warm and
54 saline Atlantic Water (AW) at intermediate depth enters the central Arctic Ocean via the deep Fram
55 Strait and the shallow Barents Sea and circulates cyclonically in the Arctic interior, controlled
56 by topography (Timmermans and Marshall 2020; Bluhm et al. 2020). The Atlantic inflow is the
57 primary heat source for the Arctic Ocean, although Pacific Water (PW) is an important source
58 of oceanic heat and relatively fresh water in the Pacific sector, especially in summer (Woodgate
59 et al. 2012). The PW contributes to the low salinity in the uppermost layer (~ 250 m) of the AB
60 (Proshutinsky et al. 2009, 2019). In contrast, in other Arctic regions, the major contributions of
61 freshwater input to the Surface Mixed Layer (SML) stem from precipitation (Serreze et al. 2006),



67 FIG. 1. Arctic Ocean map with identified regions (a). Western Eurasian basin region, Eastern Eurasian basin
 68 region, Chukchi Sea region, and Beaufort Gyre region are indicated. Light grey contour lines show the 500 m
 69 and 2000 m isobaths from ETOPO1 bathymetry (Amante and Eakins 2009). Observed annual mean depth of
 70 halocline base in the Eurasian basin (EB, red) and Amerasian basin (AB, blue) regions (b). Observed annual
 71 mean temperature (solid line) and salinity (dashed line) averaged over the halocline layer in the EB region (c)
 72 and AB region (d). Trend values are given per decade.

62 freshwater runoff from rivers (Holmes et al. 2012), glacial ice melting (Haine et al. 2015), and
 63 melting of sea ice (Haine et al. 2015; Wang et al. 2019). The Arctic Ocean’s major outflows occur
 64 through the Canadian Archipelago and the western part of Fram Strait. The Arctic Ocean’s major
 65 outflows carrying cold and fresh Polar Water (Timmermans and Marshall 2020) occur through the
 66 Canadian Archipelago and the western part of Fram Strait.

73 The volume transport and temperature of AW entering the EB have increased (Tsubouchi et al.
 74 2021; Smedsrud et al. 2022) and now play a greater role in sea ice loss in the Eurasian sector of
 75 the Arctic (Carmack et al. 2015). Although the AW inflow historically has been significant for
 76 regulating the sea ice cover in the Barents Sea and Western EB (Årthun et al. 2012; Onarheim
 77 et al. 2015), its impact on sea ice has recently expanded towards the Eastern EB; a process often
 78 referred to as “Atlantification” (Polyakov et al. 2017). Simultaneously, an anomalous advection of
 79 warm and relatively fresh PW has been observed, resulting in a recent change called “Pacification”
 80 (Polyakov et al. 2020a). The combined effect of both processes is referred to as a “Borealization”

81 (Polyakov et al. 2020a), a shift in the northward range and associated ecosystem of the Arctic
82 Ocean, which includes changes in both the physical, geochemical, and biological components.
83 The hydrographic changes related to Atlantification and Pacification are expressed regionally and
84 have opposite effects on stratification (Fig. 1 and Polyakov et al. 2020a). Pacification is mainly
85 associated with the AB and an anomalous influx of PW. Generally, anomalous advection of PW
86 makes the SML less dense and thus sharpens the density gradient and results in a strengthened
87 stratification in the AB. Atlantification has been manifested by a local surface layer salinification
88 and, therefore a weakening of the halocline and warming and shoaling of the AW layer below (Fig.
89 1 and Polyakov et al. 2020b). This results in an overall weakened stratification in the EB. These
90 conditions are more susceptible to increased vertical mixing and thus favor biological production
91 by bringing up nutrients (Polyakov et al. 2020a). Another essential local process is the general
92 freshening of the upper EB and AB (Haine et al. 2015; Haine 2020; Solomon et al. 2021), which
93 has resulted in a strengthened stratification (Li et al. 2020), especially in the AB (Polyakov et al.
94 2020a). The AB holds the largest reservoir of liquid freshwater in the Arctic, as the circulation in
95 the Beaufort Gyre, sustained by the anticyclonic winds, drives Ekman convergence and deepens
96 the halocline within the gyre (Proshutinsky 2002). Since the mid-1990s, hydrographic and satellite
97 observations have shown increases and redistribution of freshwater in the Arctic (Rabe et al. 2011;
98 Proshutinsky et al. 2019, and references therein). The increases have been linked to a combination
99 of an intensification of the large-scale atmospheric forcing over the Beaufort Gyre (Giles et al.
100 2012; Proshutinsky et al. 2019; Cornish et al. 2020), increased river runoff (Peterson et al. 2002;
101 Rabe et al. 2014; Haine et al. 2015), increased flux of freshwater through Bering Strait (Woodgate
102 et al. 2005) and direct contributions of sea ice melt (Wang et al. 2019). A recent review by Solomon
103 et al. (2021) has, however, shown that the trend in total Arctic freshwater content in the 2010s has
104 stabilized somewhat relative to the 2000s due to an increased compensation between a freshening
105 of the Beaufort Gyre and a reduction in freshwater in the rest of the Arctic Ocean. Nonetheless,
106 as the Arctic is expected to continue warming in response to our emissions (Davy and Outten
107 2020), the freshwater fluxes into to the Arctic Ocean are projected to increase (e.g. Holland et al.
108 2007; Kattsov et al. 2007; Wang et al. 2021; Jahn and Laiho 2020; Zanowski et al. 2021), partly
109 reflecting an intensification of the hydrological cycle (Held and Soden 2006; Haine 2020), and
110 partly due to increased river runoff (Haine 2020). Furthermore, freshwater contributions from sea

111 ice melt are also expected to increase in the future (Notz and SIMIP~Community 2020; Årthun
112 et al. 2021). Experiments with a column model and a global climate model show that increased
113 river runoff will strengthen the Arctic stratification (Nummelin et al. 2015, 2016). However, these
114 studies do not consider the other freshwater sources, the regional aspect, or the opposing effects of
115 Atlantification.

116 It is well known that climate models experience crucial biases in simulated Arctic hydrography.
117 This is true for both ocean-sea-ice only models (Ilicak et al. 2016; Wang et al. 2016; Tsujino
118 et al. 2020) and fully coupled climate models, such as the ones participating in the Climate Model
119 Intercomparison Project phase 5 (CMIP5; Shu et al. 2019). More specifically, the models struggle
120 to represent AW circulation and mixing processes in the Central Arctic Ocean (Ilicak et al. 2016;
121 Tsujino et al. 2020), have significant differences in circulation as a response to similar forcing
122 (Mulwijk et al. 2019), and have a large spread in projections of sea ice cover (Shu et al. 2020).
123 Despite these shortcomings, climate models are useful tools to investigate the competing processes
124 mentioned above and evaluate how they will change into the future.

125 Khosravi et al. (2022) recently published an overview of biases in the Atlantic Water layer in
126 the models that participated in the Climate Model Intercomparison Project phase 6 (Eyring et al.
127 2016, CMIP6). Their results indicate that biases persist from CMIP5 to CMIP6. Our companion
128 paper, Heuzé et al. (2022), expanded on their results by also assessing the deep and bottom waters
129 and by explaining the causes for all these biases, focusing primarily on the models' mean historical
130 state. Additionally, Arctic freshwater storage and fluxes in a subset of the CMIP6 models have been
131 analyzed by Zanowski et al. (2021), and the sea ice in CMIP6 models has been assessed by Notz and
132 SIMIP~Community (2020) and Shen et al. (2021). However, until now, no study has investigated
133 trends in stratification and hydrography regionally. We address this gap by evaluating trends in an
134 ensemble of 14 CMIP6 models. Using a unique 48-year archive of observations (1970–2017), we
135 first synthesize the observed changes in different regions of the Arctic Ocean before comparing
136 them to the historical simulations. We then describe how the stratification and hydrography in
137 these regions are projected to change under a high (ssp585) emission scenario (Eyring et al. 2016).

138 This manuscript is structured as follows: We start by describing the observational and model data
139 used in this study and present a new diagnostic used to evaluate integral changes in Arctic Ocean
140 stratification (Section 2). We then compare observed and simulated stratification in recent decades

141 (Section 3.1) before we investigate the future trends (Section 3.2 and 3.3) and finally discuss the
142 mechanisms responsible for these changes (Section 3.4 and 3.5). We focus particularly on the role
143 of advective contra local processes and finish with a summary of our findings and a discussion on
144 the broader implications of our work (Section 4).

145 **2. Data and Methods**

146 *a. Observational data*

147 This study uses a unique historical archive of hydrographic observations from 1970 to 2017,
148 including Russian, American, Canadian and European ship and aircraft expeditions, year-round
149 crewed drift stations, autonomous drifters, and submarine data. This is an updated version of the
150 archive previously used by, e.g. Polyakov et al. (2020a) to investigate long-term AW variability and
151 halocline stability. The total temporal and spatial coverage for the data used in this study is shown
152 in Fig. A1. Unfortunately, historical observations of the Arctic Ocean are generally sparse and
153 have limited spatial coverage. Especially in the 1990s, data coverage is bad, and in general, there
154 have been few winter campaigns in the central basins. However, autonomous Ice-Tethered Profilers
155 (ITP), crewed ice-drift stations, and some ship-based campaigns ensure a relatively good seasonal
156 coverage (Fig. A2). The bulk of historical data was gathered to construct the climatological
157 atlases of the Arctic Ocean by Gorshkov (1980), Treshnikov (1985), and Timokhov and Tanis
158 (1997). Before 1980 most observations used Nansen bottles to measure salinity, while modern
159 and more accurate Conductivity-Temperature-Depth (CTD) instruments became more common as
160 the use of icebreakers and submarines increased in the 1980s and 1990s. The typical accuracy
161 of measurements from the Nansen bottles was estimated by Timokhov and Tanis (1997) to be
162 0.01 °C for temperature and 0.02 for salinity. Since the 2000s, a major part of the data stems
163 from ship-based measurements complemented by drifting ITPs, which autonomously collect CTD
164 profiles down to 800 m. For consistency and direct comparison with model data we present
165 salinity and and temperature in practical salinity units (psu) and potential temperature. We use the
166 TEOS10 equation of state as implemented in the Gibbs-SeaWater (GSW) Oceanographic Toolbox
167 (McDougall and Barker 2011) to calculate density.

177 TABLE 1. Characteristics of the 14 CMIP6 models used in this study: horizontal grid type, horizontal resolution
 178 in the Arctic, type of vertical grid and number of vertical levels, ocean model component, and reference. The
 179 horizontal resolution in the Arctic (3rd column) was calculated as the square root of the total area north of 70°N
 180 divided by the number of points the model has north of 70°N. For the vertical grids, ρ means isopycnic; σ
 181 terrain-following; and multiple symbols, hybrid.

Model	Grid type	Resolution	Vertical grid	Ocean model	Reference
BCC-CSM2-MR	Tripolar	54 km	z 40	MOM4-L40v2	Wu et al. (2019)
CAMS-CSM1-0	Tripolar	54 km	z 50	MOM41	Xin-Yao et al. (2019)
CanESM5	Tripolar	50 km	z 45	NEMO3.4.1	Swart et al. (2019)
CESM2	Rotated	41 km	z 60	POP2	Danabasoglu et al. (2020)
EC-Earth3	Tripolar	49 km	z^* 75	NEMO3.6	Döscher et al. (2021)
GFDL-CM4	Tripolar	9 km	ρ - z^* 75	MOM6	Adcroft et al. (2019)
GFDL-ESM4	Tripolar	18 km	ρ - z^* 75	MOM6	Dunne et al. (2020)
GISS-E2-1-H	Regular	46 km	ρ - z - σ 32	Hycom	Kelley et al. (2020)
IPSL-CM6A-LR	Tripolar	49 km	z^* 75	NEMO3.2	Lurton et al. (2020)
MIROC6	Tripolar	39 km	z - σ 62	COCO4.9	Tatebe et al. (2019)
MPI-ESM1-2-HR	Tripolar	36 km	z 40	MPIOM1.63	Müller et al. (2018)
MRI-ESM2-0	Tripolar	39 km	z^* 60	MRI.COMv4	Yukimoto et al. (2019)
NorESM2-LM	Tripolar	38 km	ρ - z 53	BLOM (MICOM)	Seland et al. (2020)
UKESM1-0-LL	Tripolar	50 km	z^* 75	NEMO3.6	Sellar et al. (2020)

168 *b. The CMIP6 models*

169 We use the output from 14 fully coupled models that participated in the Climate Model Inter-
 170 comparison Project phase 6 (CMIP6, Eyring et al. 2016), listed in Table 1. For comparison, these
 171 models are the same as those used in our companion paper (Heuzé et al. 2022) and were selected
 172 from the 35 CMIP6 models used in Heuzé (2021) as representative of their family, for diversity in
 173 vertical grid types and after eliminating the ones with the lowest resolution or poorest bathymetry.
 174 Typical horizontal model resolution is ~ 50 km in the Arctic (9 km for the highest resolution) and
 175 50 levels or more in the vertical. No more than two models share the same ocean component with
 176 the same version (Table 1).

182 We evaluated the last 45 years of the historical run, i.e., January 1970 – December 2014, and
 183 the first 85 years of the future high (ssp585) emission scenario (Eyring et al. 2016), i.e., January
 184 2015 – December 2100. Trends were calculated from 1970–2014 to match the observational
 185 data and over 2015–2070 for the future scenario. Trends are not calculated over the full future

186 period because the changes we observe are transient, and there is some flattening towards the
187 end of the century (Section 3b). For each model, only one ensemble member was used. All
188 trends presented are statistically significant unless otherwise stated. The output we used are the
189 monthly seawater practical salinity “so” and potential temperature “thetao”. Density was calculated
190 using the TEOS10 equation of state as implemented in the Gibbs-SeaWater (GSW) Oceanographic
191 Toolbox (McDougall and Barker 2011). All computations were performed on the models’ native
192 grid before being averaged for each of the four regions shown in Fig. 1.

193 *c. Methods*

194 The primary objective of this paper is to quantify trends in stratification. Traditionally, strat-
195 ification has been quantified using the Brunt-Väisälä buoyancy frequency $N^2 = -(g/\rho_0)\delta\rho/\delta z$,
196 where ρ is potential density, ρ_0 is a reference density, and g is the gravitational acceleration. This
197 parameter provides a profile of stability between points in the vertical but does not yield a bulk
198 measure of the stability within a layer (Polyakov et al. 2018). The upper part of the EB and AB
199 water column features complex layering. It consists of a surface mixed layer (SML, $\sim 20\text{--}50$ m)
200 overlaying the halocline, characterized by cold temperatures and a very high salinity gradient (\sim
201 $50\text{--}250$ m), and a warmer (temperature $> 0^\circ\text{C}$) and more saline layer of AW below (Rudels et al.
202 2004). Traditionally, the definition of AW is based on temperature, salinity, or density values.
203 However, since we expect these properties to be biased in the models, we instead chose to define
204 the Atlantic Water core as the depth of the temperature maximum below 100 m, similar to what is
205 done by Heuzé et al. (2022). When we further refer to AW properties, we thus mean the properties
206 at the depth of the AW core. According to Heuzé et al. (2022), the CMIP6 multi-model mean
207 AW core depth is approximately 400 m in the EB and approximately 530 m in the AB but varies
208 substantially from model to model (ranging between 77 m and 1300 m).

209 The halocline is often divided into a cold halocline, with near-freezing temperatures, and lower
210 halocline waters, with increasing temperature and salinity with depth (Steele et al. 1989; Rudels
211 et al. 2004). Polyakov et al. (2018) noted that, especially within the halocline, which consists of
212 a complex combination of water masses with varying effects on stratification (Bluhm et al. 2015),
213 N^2 is insufficient as a measure of stratification since it does not provide a bulk metric. Also, a
214 simple density contrast between two levels ($\Delta\sigma_\theta$) is similarly insufficient. Polyakov et al. (2018)

215 therefore proposed Available Potential Energy (APE) as a good integral indicator of changes in
 216 stratification in the combined SML and halocline layer. For each profile, APE is calculated as:

$$APE = \int_{H_{halo}}^{surface} g(\rho - \rho_{halo})zdz, \quad (1)$$

217 where H_{halo} is the depth of the lower boundary of the halocline and ρ_{halo} is the potential density
 218 at that lower boundary of the halocline.

219 In observations, the lower boundary of the halocline is usually determined using a density ratio
 220 algorithm following the method proposed by Bourgain and Gascard (2011), which was also used
 221 by e.g. Polyakov et al. (2018) and Metzner et al. (2020). Following Bourgain and Gascard (2011),
 222 such density ratio is defined as

$$R_\rho = \left| \left(\alpha \frac{\delta\Theta}{\delta z} \right) / \left(\beta \frac{\delta S_A}{\delta z} \right) \right| \quad (2)$$

223 where α is the thermal expansion coefficient, β is the haline contraction coefficient, Θ is the
 224 conservative temperature, and S_A is the absolute salinity. The lower boundary of the halocline
 225 H_{halo} is then defined as the depth where R_ρ exceeds the threshold of 0.05, which was determined
 226 empirically from observations in the Arctic (Bourgain and Gascard 2011).

227 In general, models struggle to reproduce the Arctic halocline properly (Nguyen et al. 2009), and
 228 large temperature and salinity biases in the Arctic Ocean (Heuzé et al. 2022) make it difficult to
 229 properly define the halocline using the same criteria as in the observations. Manually deriving
 230 model-specific definitions is not ideal either, as the biases might vary over time. We, therefore,
 231 find that the uncertainty of properly defining the “correct” halocline in CMIP6 models based on
 232 Equation (1) is too high and have chosen to investigate Arctic stratification in CMIP6 models using
 233 an indicator whose definition is less dependent on defining a halocline.

234 We therefore first define the potential energy of the water column following Tailleux (2009) as:

$$PE(H) = \int_H^{surface} g(z)\rho(z)zdz \quad (3)$$

235 where H is a chosen depth level. We then look at the difference in potential energy between the
 236 simulated stratified water column and a fully mixed water column, which reflects the energy needed

237 to fully mix the water column from the surface to a given depth:

$$\Delta PE(H) = PE(H) - PE(H)_{mixed}. \quad (4)$$

238 We define $\Delta PE(H)$ as the *work* required to overcome stratification (hereafter referred to as “*work*”) since $PE(H)_{mixed}$ represents the potential energy of a completely mixed water column with a mean temperature and salinity down to depth H . We note that this quantity describes a process of irreversible mixing, whereas APE describes the difference to adiabatically rearranged minimum energy, which would be reversible. *Work* can thus be seen as an idealized measure of the strength of stratification where a higher *work* value reflects a stronger stratification down to a certain depth.

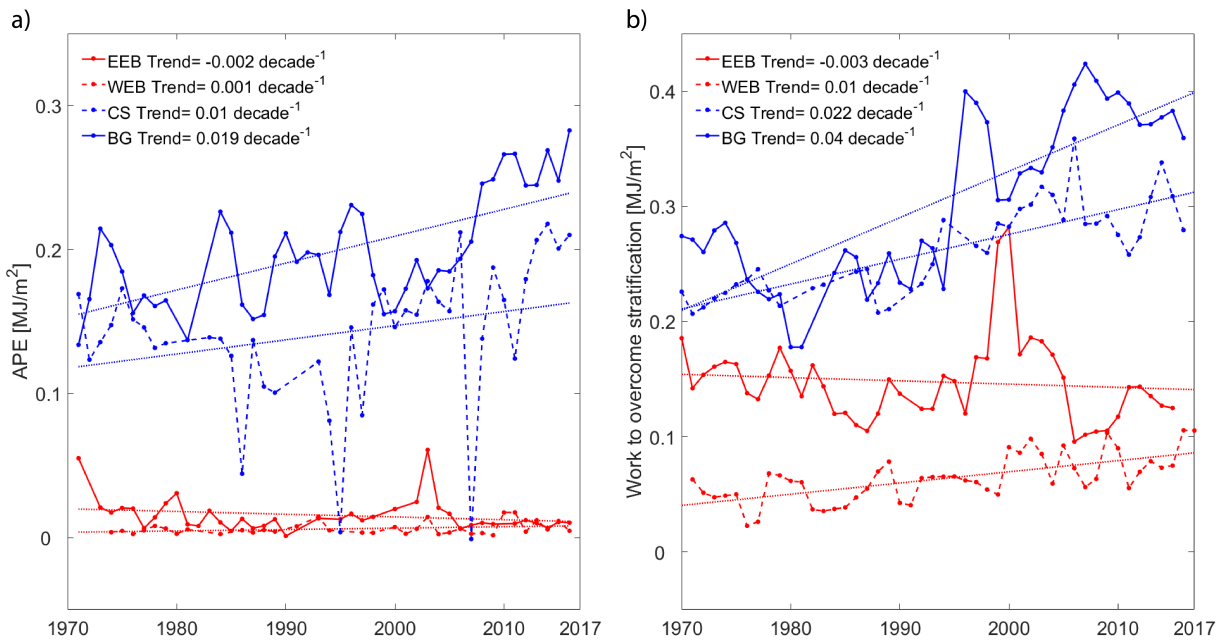
244 As long as H is well below the typical halocline depth, we show that APE and *work* capture similar changes and are equally good indicators of stratification strength in the Arctic Ocean. However, *work* is preferred in models as its definition is independent of temperature and salinity gradients. A comparison of the two parameters is given in Section 3a. We use *work* from $H = 300$ m (well below the halocline according to Heuzé et al. 2022) as our main indicator of stratification strength in the models and hereafter refer to changes in *work* as changes in stratification.

250 3. Results

251 a. Recent decades (1970–2014)

252 1) OBSERVED STRATIFICATION CHANGES

253 We start by analyzing hydrographic observations from four regions in the Arctic Ocean (Fig. 1); two in the AB (Beaufort Gyre and the Chukchi Sea) and two in the EB (Western and Eastern EB), consistent with previous studies (e.g. Polyakov et al. 2020a). The halocline base is deeper in the AB (~ 200 m) than in the EB (~ 90 m, Fig. 1). Since 1970 it has deepened in the AB (~ 7 m decade $^{-1}$) and shoaled in the EB (~ 3 m decade $^{-1}$), although the latter trend is not statistically significant. In the AB, the halocline freshens (~ 0.11 psu decade $^{-1}$), which other studies have documented (Carmack et al. 2016; Proshutinsky et al. 2019; Polyakov et al. 2020a). The EB halocline shows overall no statistically significant salinity trend, although a moderate salinification has been observed in the Eastern EB region in recent decades (Polyakov et al. 2020a, not shown here). The Eastern EB salinification and AB freshening were recently taken as indicators of the



268 FIG. 2. Observed annual mean stratification within the Arctic Ocean using two different measures. Regions are
 269 shown in Fig. 1. a) available potential energy APE following equation (2), and b) *work* to overcome stratification
 270 ($\Delta PE(H)$) from 300 m following equation (4). Blue colors are used for the AB, and red colors are used for EB.
 271 WEB = Western Eurasian basin, EEB = Eastern Eurasian basin, CS = Chukchi Sea and BG = Beaufort Gyre. In
 272 a) only the BG trend is statistically significant ($p \geq 0.05$), whereas in b) all trends, except the EEB, are statistically
 273 significant.

263 ongoing Atlantification and Pacification (Polyakov et al. 2020a), but we note that particularly
 264 Pacification is difficult to distinguish from the local freshening occurring in the upper Arctic Ocean
 265 due to increased runoff or precipitation. Alongside the halocline freshening in the AB, there is
 266 general warming ($\sim 0.04 \text{ }^\circ\text{C decade}^{-1}$) related to PW inflow (Polyakov et al. 2020a). Also, the
 267 halocline warms ($\sim 0.04 \text{ }^\circ\text{C decade}^{-1}$), but again, these trends are not statistically significant.

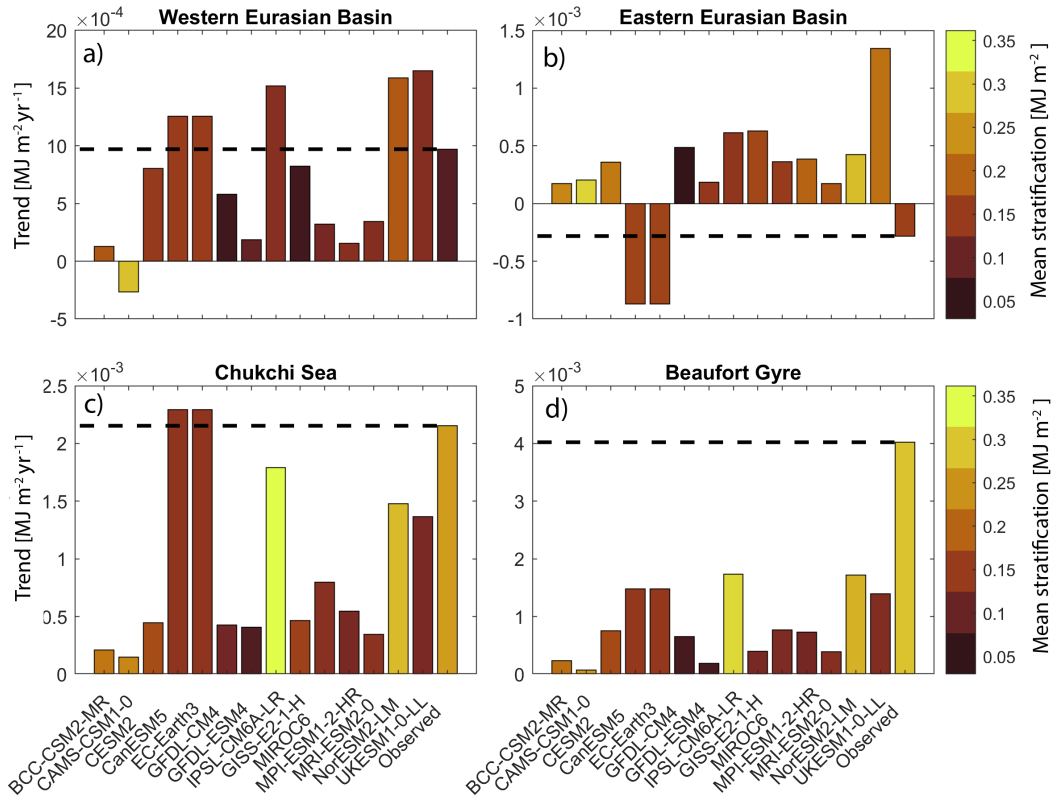
274 The contrasting changes in upper ocean salinity and temperature in the EB and AB result in
 275 different effects on the regional halocline stability and thus stratification. In Fig. 2a, we present
 276 the regional time series of APE, following Equation (2) and Polyakov et al. (2018). By definition,
 277 APE is directly linked to halocline base depth and is, therefore, an order of magnitude larger in the
 278 AB than in the EB. There is a strong positive trend in APE in the Chukchi Sea and Beaufort Gyre,
 279 which is associated with a strengthening of the stratification (Fig. 2a). A weaker but still positive

280 trend is also evident in the Western EB region (not statistically significant). In contrast, the APE in
281 the Eastern EB shows a (not statistically significant) negative long-term trend. These findings are
282 consistent with (Polyakov et al. 2018) who showed that the most considerable changes in Arctic
283 Ocean stratification have occurred in the AB and other studies which show that the halocline has
284 weakened in the EB towards the end of the twentieth century (Steele et al. 1989; Polyakov et al.
285 2017, 2020b).

286 Time series of “work to overcome stratification” ($\Delta PE(H)$), hereafter referred to as “work”) are
287 calculated following Equations (3) and (4) (Fig. 2b). We use the observational time series to
288 illustrate that, ultimately, APE and *work* are qualitatively equal and comparable measures of the
289 integrated upper-ocean stratification. APE shows that the *work* required to overcome stratification
290 strongly increases in the Beaufort Gyre and Chukchi Sea regions and moderately increases in the
291 Western EB. In the Eastern EB, *work* has a negative trend, meaning the stratification is weakened.
292 In the following section, we compare the observed changes in stratification to simulations from 14
293 CMIP6 models.

294 2) SIMULATED STRATIFICATION CHANGES

295 On average, most models analyzed in this study are less stratified in the Arctic Ocean than
296 observations show (colors of bars in Fig. 3), as also discussed by Heuzé et al. (2022). Notable
297 exceptions in the Eurasian Basin (top panels Fig 3) are CAMS-CSM1-0 and NorESM2-LM, with
298 mean stratification exceeding 0.3 MJ m^{-2} , i.e., three times the observational values. NorESM2-LM
299 is also more stratified than observations in the Amerasian Basin (bottom panels, Fig. 3), but IPSL-
300 CM6A-LR is the one overestimating stratification the most with a value of 0.36 MJ m^{-2} . That is,
301 biases in stratification are not consistent throughout the Arctic in CMIP6 models. Moreover, most
302 models do not correctly represent the difference in stratification between the two basins and instead
303 have similar values throughout the Arctic (i.e., the same color of bars on all panels of Fig. 3), a
304 result consistent with the biases in water mass properties described in Heuzé et al. (2022). In fact,
305 all models except GFDL-CM4 and IPSL-CM6A-LR are incorrectly more stratified in the eastern
306 EB than in the AB. CAMS-CSM1-0, CanESM5, EC-Earth3, GFDL-ESM4 and MPI-ESM1-2-HR
307 are more stratified in the western EB than in the AB, as well. It is worth noting that no model is



310 FIG. 3. Simulated trends in *work* to overcome stratification for each of the CMIP6 models listed in Table 1 from
 311 1970–2014. Dashed black lines and rightmost bars indicate the observed trends (Fig. 2), and color bars indicate
 312 the mean stratification strength in different regions for each model. Note the different y-axes on all panels.

308 too strongly biased to not be kept in this study, i.e., all stratification values are in the same order of
 309 magnitude as the observations.

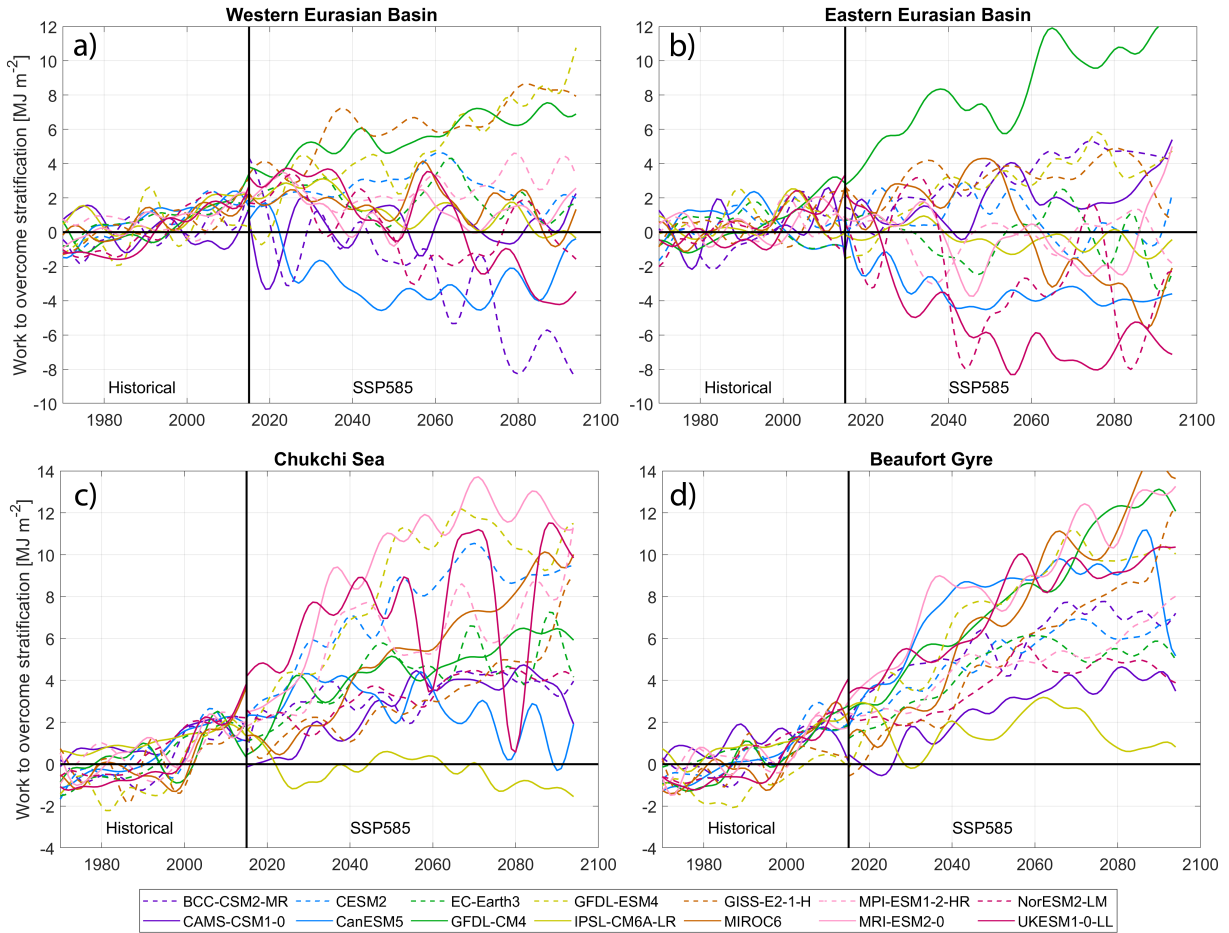
313 In accordance with observations, all models show a positive trend in stratification (strengthening)
 314 in the AB over the period 1970–2014 (Fig. 3, length of the bars). However, the absolute values
 315 of the trends are much lower than in the observations. There appears to be no clear relationship
 316 between the mean strength of stratification and the magnitude of trends (Fig. A3). The models
 317 also agree on a larger change in stratification in the AB compared to the EB. Only CAMS-
 318 CSM1-0 produces a weakened stratification in the Western EB, while all other models simulate
 319 a strengthened stratification similar to the observed trend. In the Eastern EB, there is a larger
 320 disagreement among the models, both in the mean state and in their trends, and only two models
 321 (CanESM5 and EC-Earth3) simulate a weakened stratification there, as observed from 1970-2014
 322 (Fig. 2 b). In other words, only two models reproduce an Atlantification (as diagnosed through

323 APE/*work*) comparable to what has been observed. In the next sections, we investigate how these
324 trends are projected to continue or change into the future and how this is related to the hydrographic
325 structure in the various regions and models.

326 *b. Future trends in stratification*

327 The temporal anomalies of the simulated *work* required to overcome stratification relative to
328 the historical period (1970–2014) show significant variations in the various regions both in the
329 historical period and under the ssp585 forcing scenario (Fig. 4). Within the EB, the models diverge
330 regarding future stratification. Fig 4 shows large differences among the models, with the largest
331 intermodel spread in the Eastern EB. Some models project a clear increase in EB stratification
332 (e.g., GFDL-CM4, GFDL-ESM4, GISS-E2-1-H, and CAMS-CSM1-0) while others project a clear
333 decrease (e.g., UKESM1-0-LL, CanESM5, NorESM2-LM, and IPSL-CM6A-LR). Despite only
334 two models showing an indication of Atlantification in the period 1970–2014, approximately half
335 of the models predict a future weakening of the EB stratification and thus Atlantification. Despite
336 the large spread in the EB, there is agreement among the models (except IPSL-CM6A-LR, plain
337 yellow line) on an increased future stratification in the Chukchi Sea and Beaufort Gyre regions.
338 This means that the observed strengthening of the halocline in the AB is projected to continue
339 and amplify into the future. In the Beaufort Gyre, the trends continue throughout the twenty-first
340 century, whereas in the Chukchi Sea, the curve flattens in the 2060s for many of the models, albeit
341 with strong interannual variability.

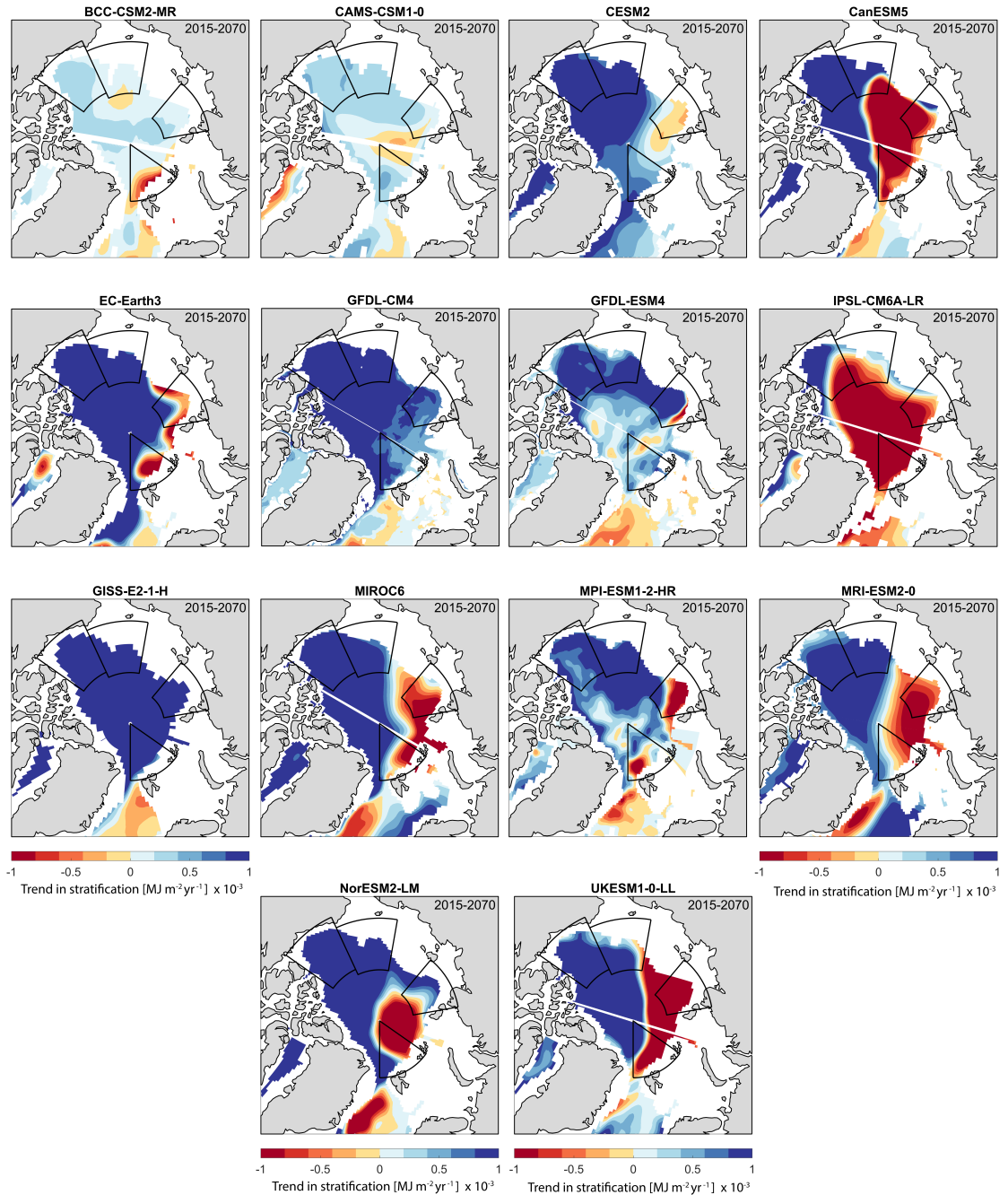
348 The average future trend in stratification also varies spatially for the selected models (Fig. 5).
349 There is a clear division and opposite trends in the AB and EB, similar to what has been documented
350 by Polyakov et al. (2020a). The opposing trends can be understood as the competing influences of
351 the Atlantic and Arctic domains. All models show a weakening of stratification in some parts of the
352 EB (red colors) and a strengthening of stratification in most parts of the AB (blue colors). However,
353 the exact location, extent, and magnitude of the Atlantification signal varies, resulting in a large
354 spread, especially in the Eastern EB. Interestingly, for most models, the indicated Atlantification is
355 mainly confined towards the Eastern parts of the EB and the Barents Sea outflow near the St. Anna
356 trough and less towards Fram Strait. It is possible that because AW is in closer contact with sea ice
357 north of Svalbard, more sea ice is melted there, resulting in increased surface freshening and hence



342 FIG. 4. Regional time series of normalized (anomalies relative to 1970–2014 model mean) *work* to overcome
 343 stratification $\Delta PE(H)$ for the 14 CMIP6 models listed in Table 1. All time series are low-pass filtered with a
 344 five year cutoff-frequency. Note the different y-axes for the two basins.

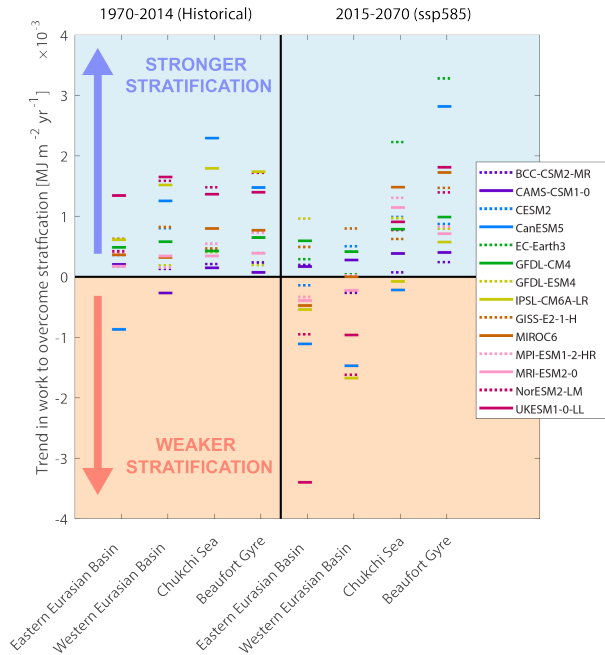
358 a strengthening of the stratification. GISS-E2-1-H is the only model that shows no indication of
 359 Atlantification, whereas IPSL-CM6A-LR, CanESM5, and UKESM1-0-LL show the largest spatial
 360 extent of Atlantic influence.

361 We quantify and summarize the historical and future trends for each region in Fig. 6. The
 362 dipole-like pattern is also clearly illustrated here, with obvious differences between the evolution
 363 of the EB and AB. The spread amongst the models is comparable in both basins ($\sim 3 \text{ MJ m}^{-2} \text{ yr}^{-1}$),
 364 but this spread results in opposite signs in the EB, whereas, as shown previously, most models
 365 project an increase in stratification in the AB. The future trends in the AB are somewhat larger
 366 than the historical trends. More than half of the models show a strong weakening trend in the EB,



345 FIG. 5. Future spatial trends in *work* to overcome stratification $\Delta PE(H)$ under a strong greenhouse-gas forcing
 346 scenario (ssp585) for the 14 CMIP6 models listed in Table 1. Negative values mean a weakening of stratification.
 347 All trends are annual means calculated over the period 2015-2070.

367 with CanESM5, NorESM2-LM, IPSL-CM6A-LR, and UKESM1-0-LL having the largest changes.
 368 UKESM1-0-LL is an extreme in the Eastern EB with a trend four times stronger than any other



373 FIG. 6. Mean regional trends in *work* to overcome stratification $\Delta PE(H)$ for our 14 CMIP6 models. The
 374 trends over the historical period (1970-2014) are shown on the left, and the trends over the future period (2015-
 375 2070) under a strong greenhouse-gas forcing scenario (ssp585) are shown on the right. As in Fig. 5, positive
 376 values (blue shading) denote increased stratification, and negative values (orange shading) denote weakened
 377 stratification.

369 model. These changes in stratification can be the result of changes in the upper ocean (SML and
 370 halocline) and water masses below the halocline, such as the AW. In the following section, we
 371 examine what drives the changes in stratification in the various regions and focus on the difference
 372 between the surface and AW layers.

378 *c. Atlantic Water and surface trends*

379 We showed that the models diverge when predicting changes in stratification in the EB and
 380 show a large spread in the AB. These changes could be primarily driven by changes in surface
 381 water masses or changes in the AW layer. We assume that most changes at the surface are driven
 382 by local processes (e.g., sea ice melt/growth, river runoff, evaporation-precipitation, surface heat
 383 fluxes, etc.), and those in the AW layer are advected in through the Fram Strait and the Barents
 384 Sea, and mainly related to processes beyond the boundaries of the Arctic Ocean. The question

390 TABLE 2. Future Atlantic Water core (temperature maximum below 100 m) temperature and salinity trends for
 391 each of the CMIP6 models (forcing scenario ssp585) over 2015–2070. Values are given in °C decade⁻¹ and psu
 392 decade⁻¹. Statistically non-significant trends ($p \geq 0.05$) are shown in italic.

	Western EB		Eastern EB		Chukchi Sea		Beaufort Gyre	
	θ	S	θ	S	θ	S	θ	S
BCC-CSM2-MR	.013 ± .004	-.016 ± .005	-.002 ± .000	.003 ± .001	-.002 ± .000	-.004 ± .000	-.003 ± .000	-.004 ± .000
CAMS-CSM1-0	.032 ± .008	.015 ± .002	.012 ± .001	-.005 ± .001	.001 ± .001	-.015 ± .001	.006 ± .001	-.008 ± .002
CESM2	.355 ± .018	-.062 ± .007	.310 ± .013	-.047 ± .005	.224 ± .012	-.043 ± .002	.115 ± .010	-.045 ± .002
CanESM5	.729 ± .026	-.036 ± .004	.428 ± .021	-.082 ± .006	.454 ± .029	-.040 ± .006	.525 ± .029	-.017 ± .004
EC-Earth3	.606 ± .024	.028 ± .004	.470 ± .013	.011 ± .005	.429 ± .031	.056 ± .003	.225 ± .033	.041 ± .004
GFDL-CM4	.143 ± .005	-.021 ± .001	.120 ± .005	-.020 ± .002	.176 ± .010	-.009 ± .001	.088 ± .007	-.008 ± .001
GFDL-ESM4	.097 ± .018	-.032 ± .002	.152 ± .009	-.026 ± .001	.121 ± .008	-.024 ± .001	.061 ± .005	-.005 ± .001
IPSL-CM6A-LR	.402 ± .023	-.004 ± .005	.301 ± .021	-.018 ± .006	.330 ± .028	-.012 ± .007	.360 ± .023	-.020 ± .007
GISS-E2-1-H	.040 ± .007	.004 ± .007	.155 ± .008	.000 ± .005	.155 ± .002	-.009 ± .002	.125 ± .005	-.009 ± .002
MIROC6	.286 ± .019	-.092 ± .003	.122 ± .014	-.091 ± .003	.162 ± .004	-.072 ± .003	.144 ± .004	-.063 ± .004
MPI-ESM1-2-HR	.314 ± .016	-.015 ± .002	.105 ± .016	-.038 ± .002	.242 ± .019	-.016 ± .001	.301 ± .014	-.009 ± .001
MRI-ESM2-0	.444 ± .012	-.094 ± .004	.291 ± .013	-.093 ± .003	.268 ± .015	-.100 ± .003	.207 ± .016	-.092 ± .005
NorESM2-LM	.346 ± .017	-.063 ± .005	.171 ± .024	-.118 ± .005	.312 ± .020	-.096 ± .004	.299 ± .022	-.090 ± .005
UKESM1-0-LL	.740 ± .028	-.009 ± .005	.713 ± .024	-.038 ± .008	.735 ± .024	-.030 ± .008	.604 ± .036	-.035 ± .006

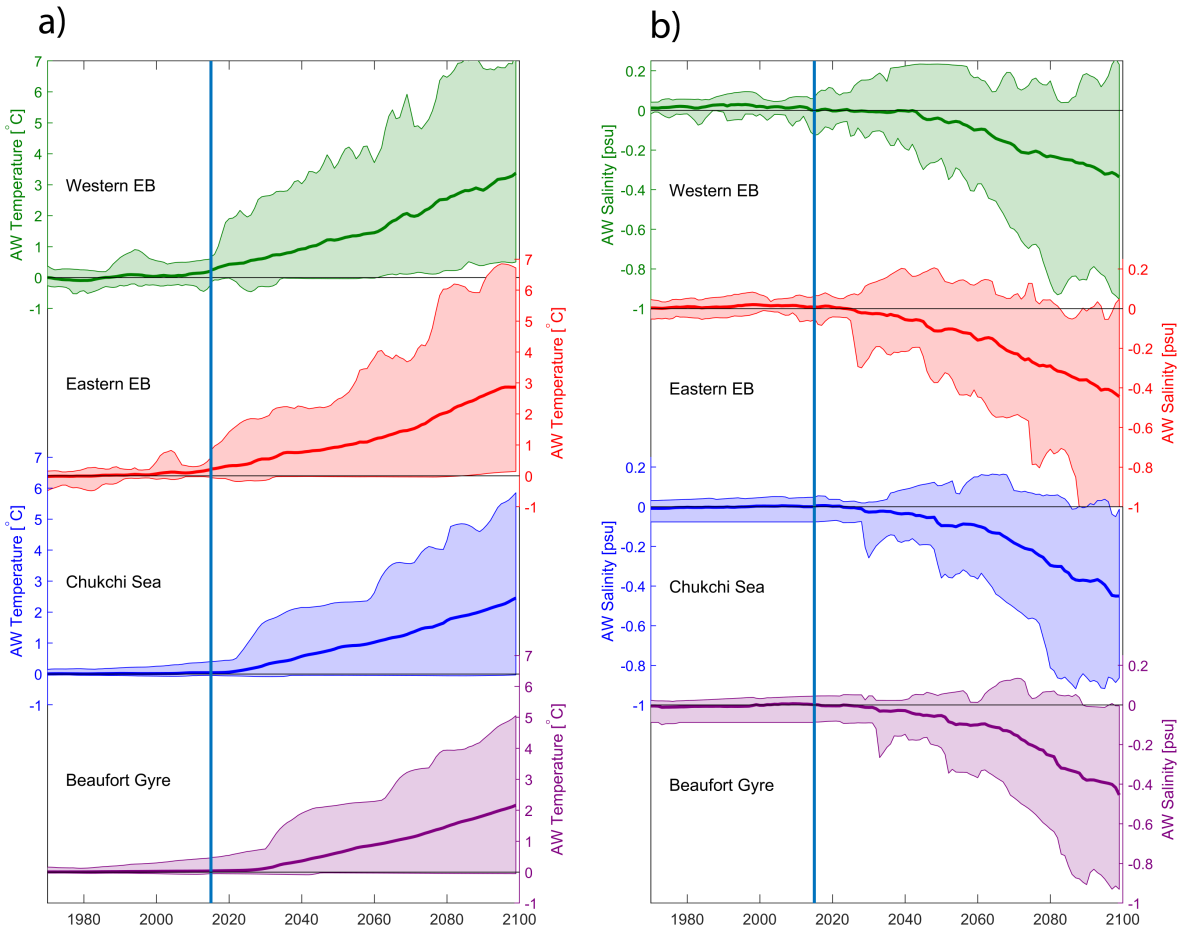
385 then becomes: are the simulated changes in stratification mainly locally driven or remotely forced?
 386 Of course, the layers are not fully disconnected, and mixing occurs along the AW pathways, but
 387 Heuzé et al. (2022) revealed that in the CMIP6 models, there is a strong decoupling between the
 388 upper layer and the rest of the deep Arctic (below 200 m). This is partly attributed to an absence of
 389 ventilation, and as a result, the properties of the Arctic AW layer are closely linked to the inflows.

393 We start by detailing the evolution of AW core temperature and salinity in the four different
 394 regions. As expected, with continued global warming, the AW temperature is projected to increase
 395 in all regions by all models (Fig. 7). Thick lines in Fig. 7 represent the multimodel mean
 396 anomalies relative to each model’s historical mean, and colored envelopes indicate the minimum
 397 and maximum of the model spread per time step. A full overview of the property trends in the
 398 various models is presented in Table 2. We note that AW core properties are calculated based
 399 on each model’s AW core depth (details in Section 2c), which varies substantially from model to
 400 model (Heuzé et al. 2022). The models project an increase in AW temperature with a range of
 401 0–7 °C relative to the historical mean towards the end of the 21st century. The AW temperature

402 change is relatively linear over time and reaches a multi-model mean increase of 3.0 °C in the EB
403 and 2.5 °C in the AB by 2100. Some models predict very weak trends in AW temperature, but the
404 majority predict strong warming, in accordance with what was shown by Khosravi et al. (2022).
405 Less intuitive, perhaps, is the future change of AW salinity. Most models simulate a freshening
406 of the AW layer throughout the Arctic (Table 2), except EC-Earth3 which simulates an increase
407 in AW salinity in all regions. Averaged across the regions, the multi-model mean freshening is
408 approximately 0.5 psu by the end of the century.

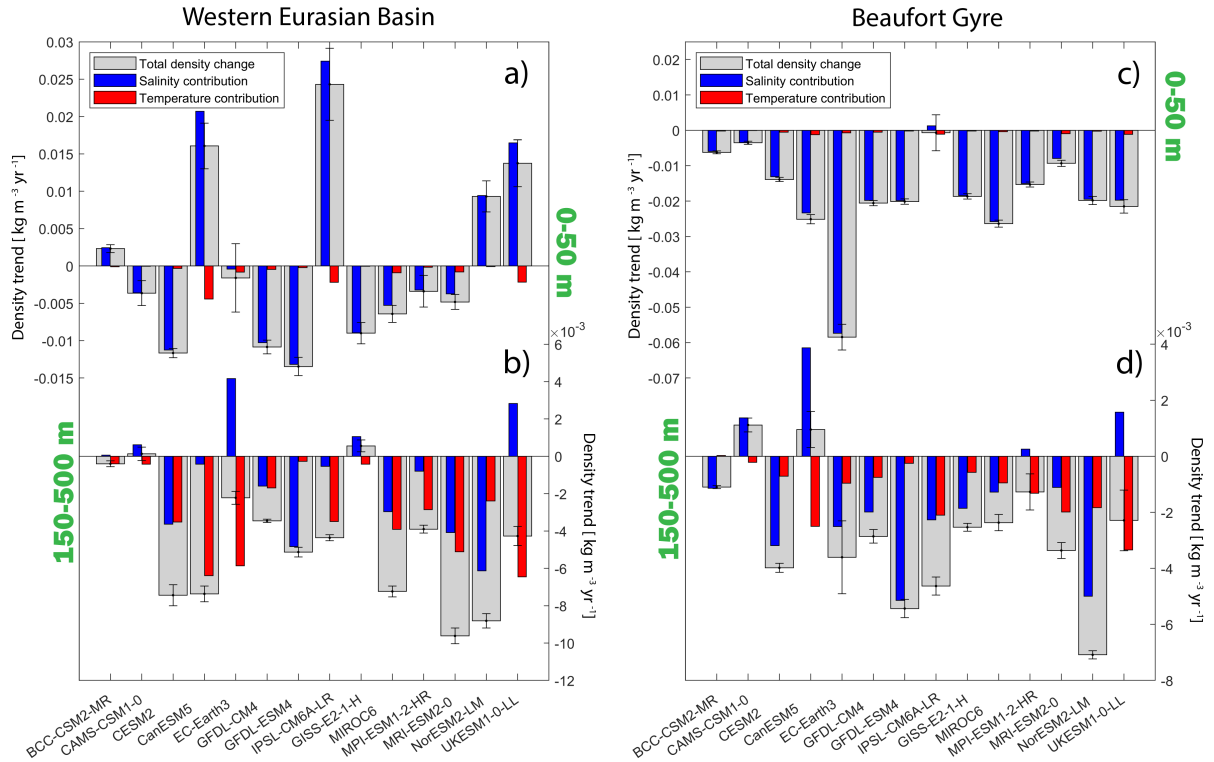
414 The decrease in AW salinity indicates that the northward freshwater flux through the Fram Strait
415 and Barents Sea Opening increases, which is consistent with results from Zanowski et al. (2021).
416 Over 2015-2070 all models, except CAMS-CSM1-0 and GFDL-CM4, show a positive trend in the
417 liquid freshwater flux through the Barents Sea opening, which mainly consists of northward-flowing
418 AW (Fig. A4b). The freshwater flux through Fram Strait is more complex, as it consists of both a
419 southward and a northward flow. Here we observe a negative trend in the (northward) freshwater
420 flux (Fig. A4a), meaning an increase in the net southward freshwater flux. This makes sense, as
421 the increase in the outflowing freshwater is larger than the increase in the inflowing freshwater (as
422 it also includes the other freshwater sources). All in all, a decrease in the northward-flowing AW
423 contributes to a freshening at intermediate depths and ultimately an increase in the total freshwater
424 content of the Arctic and the southward export of freshwater, as also shown by Zanowski et al.
425 (2021). Our findings stress an important point that has not been stated in current literature, namely
426 that the future freshening of the Arctic Ocean may be attributed to both surface and AW forcing
427 and is thus both locally and remotely driven.

432 As we continue with the temperature and salinity evolution of the surface layer (0–50 m), different
433 model behaviors become even more evident (Table A1). In the AB, all models project a freshening
434 and warming of the surface layer, consistent with current observations (Solomon et al. 2021)
435 and the expected continuation of AB freshening (Haine 2020). Averaged across the models, the
436 absolute change in surface salinity is expected to reach approximately -1.5 psu by the end of the
437 century (Fig. A5). In the EB, on the other hand, many models project a freshening, but some
438 project a surface salinification (Fig. A5). Some of the models that project a surface salinification
439 are the same that project an AW salinification (Fig. 8), but for others, there are opposite trends
440 in the AW and surface layers. There is no consistent relationship between the direction of surface



409 FIG. 7. Regional time series of normalized (reduced to anomalies relative to 1970–2014 model mean) Atlantic
 410 Water core temperature (a) and Atlantic Water core salinity (b) from the CMIP6 models listed in Table 1. Thick
 411 lines represent the multimodel mean, and envelopes show the minimum and maximum of the model spread per
 412 time step. The Atlantic Water core properties are calculated as the properties at the temperature maximum below
 413 100 m.

441 trends and trends in the AW layer, and there is also no clear relationship between changes in
 442 AW/surface properties and freshwater/salinity fluxes through the Fram Strait and the Barents Sea
 443 (not shown). The multi-model mean still projects a freshening in both the Eastern and Western
 444 EB, although some models have opposing trends. Figs. 7 and A5 emphasize the importance of the
 445 regional aspect when investigating future Arctic Ocean change. Even though the general change
 446 is similar (AW warming and freshening), the regions are projected to evolve somewhat differently



428 FIG. 8. Trends in density in the upper ocean (a) and c)) and at intermediate depth (b) and d) for the Western
 429 Eurasian basin (left) and the Beaufort Gyre region (right) for each of the CMIP6 models listed in Table 1. Red
 430 and blue bars denote the relative contributions of temperature and salinity trends to the total density trends (thick
 431 grey bars). Positive values mean increased density, and negative values mean decreased density.

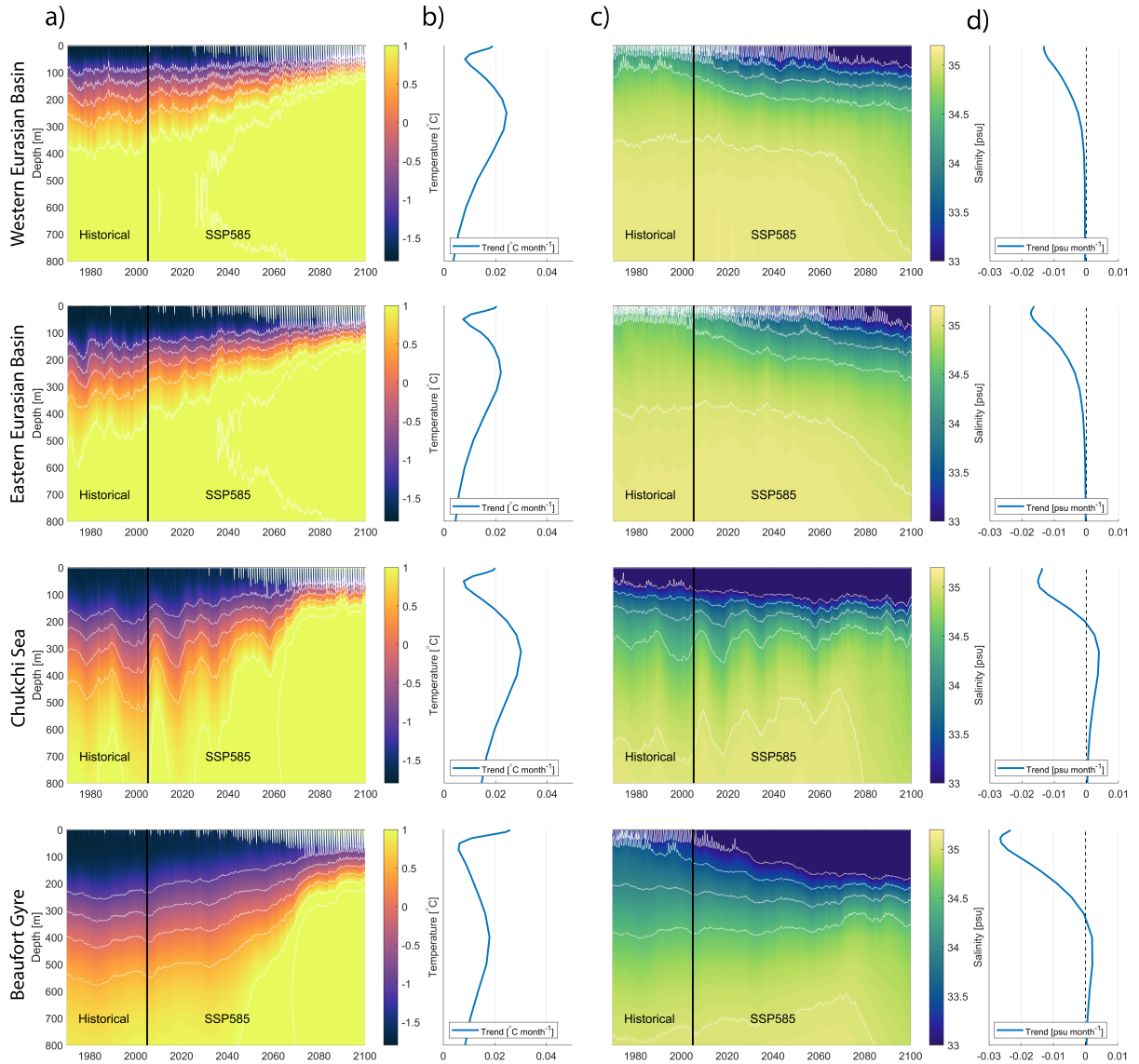
447 or on different timescales. For example, the Eastern and Western EB are exposed to different
 448 processes as they have a different seasonal ice cover, which is projected to change differently in
 449 the future (Notz and SIMIP~Community 2020). Taking a Eurasian basin or Canadian basin mean,
 450 as is common practice in CMIP studies of the Arctic Ocean, is therefore not ideal since one might
 451 lose important information and average out important regional differences.

452 Differences in salinity and temperature trends result in different contributions to the overall
 453 density profile. Fig. 8 shows the comparison of density changes in the upper ocean (0–50 m,
 454 lower per panel) and at intermediate depth below the halocline (150–500 m, lower panel) for each
 455 model in the Western EB and the Beaufort Gyre regions (The Eastern EB and Chukchi regions are
 456 shown in Fig. A6). Red and blue bars denote the relative contributions of temperature and salinity
 457 trends to the total density trends (fat grey bars), respectively. Note the different scales on the

458 y-axis. In the upper ocean, the density changes are mainly driven by salinity changes. In contrast,
459 at intermediate depth, the density changes are more equally attributed to both temperature and
460 salinity. In some cases, temperature and salinity have opposite effects (EC-Earth3 and UKESM1-
461 0-LL), and the contribution from warming is slightly larger than the salinification, resulting in
462 an overall decrease in AW density. In other cases, for example in CAMS-CSM1-0, salinification
463 overpowers the warming. In general, the upper ocean density trends are much larger than the
464 trends at intermediate depth, meaning that the stratification changes are mainly driven by changes
465 at the surface. Opposing results in the EB stratification are primarily related to opposite changes in
466 surface density (Fig. 8a). However, density trends further down in the water column also contribute
467 and may either enhance or diminish the impact of the surface trend on the overall stratification.
468 For example, in the Western EB, changes in the surface and AW layer in CanESM5 contribute to
469 a weakening of the stratification. In CESM2, on the other hand, the surface trends contribute to
470 a strengthening of the stratification, and the intermediate layers contribute to a weakening of the
471 stratification. In summary, the relative change between the upper ocean and intermediate layer
472 ultimately determines whether the density gradient increases or decreases. We detail these vertical
473 density gradients and how they change over time in the following section.

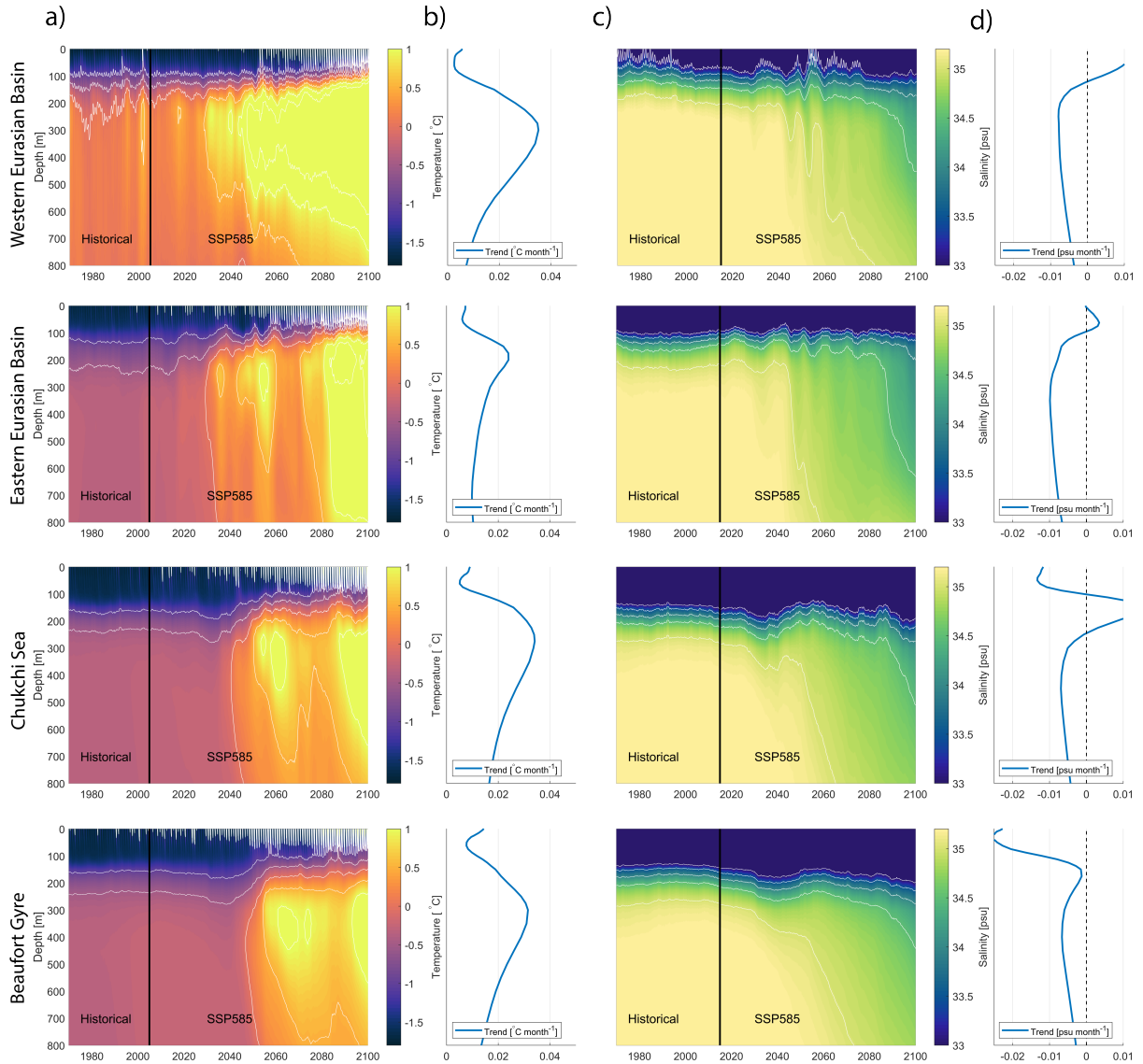
474 *d. Future density gradients*

475 We compare two models, GFDL-CM4 and NorESM2-LM, which project distinctly opposite
476 changes in stratification in the EB (Fig. 6). In Fig. 9 we present the temporal development of
477 temperature and salinity profiles for the GFDL-CM4 model, which projects a strengthening in
478 stratification in all regions. Profiles shown in columns b) and d) represent the linear trends in
479 temperature and salinity at each depth level over 2015–2070. The temperatures are projected to
480 increase throughout the whole water column, but the change is largest between 200–500 m and
481 smallest in the halocline, just below the surface mixed layer. These trend profiles might not solely
482 be due to a change in properties at the given depths but are also a result of the upward or downward
483 movement of the AW and/or a deepening or shoaling of the SML. Due to space limitations, we
484 do not investigate these changes in this paper, but Khosravi et al. (2022) give a good overview of
485 changes in AW core depth and changes in SML depth; the processes related to this will be studied
486 in detail in a follow-up paper.



487 FIG. 9. Monthly mean upper ocean temperature (a) and salinity (c) from GFDL-CM4 from 1970 to 2100
 488 for each region identified in Fig. 1. Linear trends are calculated for each depth level from 2015 to 2070 for
 489 temperature (b) and salinity (d).

493 The salinity trend profiles (Fig. 9 d) show the largest trends at the surface, which gradually
 494 decreases with depth. In this model, below 300 m, there is almost no change in salinity, despite a
 495 small positive trend in AW salinity in the AB regions. This is thus an example of a model where
 496 upper ocean salinity changes primarily drive the stratification changes. These projections appear
 497 plausible, and we can relate the changes to known mechanisms. However, this is a good example

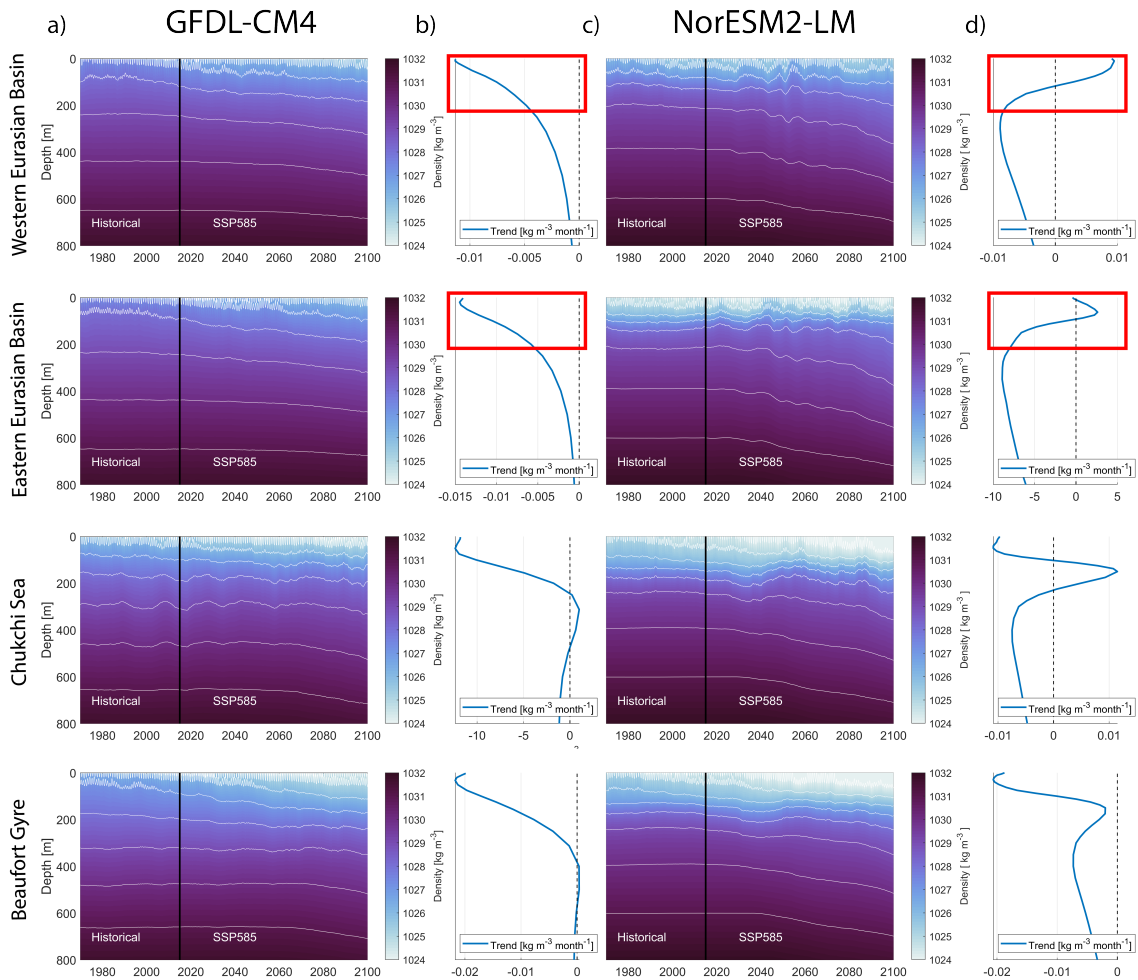


490 FIG. 10. Monthly mean upper ocean temperature (a) and salinity (c) from NorESM2-LM from 1970 to 2100
 491 for each region identified in Fig. 1. Linear trends are calculated for each depth level from 2015 to 2070 for
 492 temperature (b) and salinity (d).

498 of why it is dangerous to conclude future Arctic Ocean changes based on a single model system:
 499 A study based on a different model system may provide an opposite result. Fig. 10 shows the
 500 temperature and salinity trend profiles for NorESM2-LM, a model which shows a weakening of
 501 the stratification in the EB and a strengthening of stratification in the AB. Overall, the vertical
 502 distribution of temperature trends looks very similar between NorESM2-LM and GFDL-CM4,

503 which is true for all other models (not shown). Although the absolute values (and mean states) vary
504 from model to model, they all simulate a positive temperature trend throughout the whole water
505 column, with a maximum around 200 m depth and a minimum just below the SML. However, the
506 salinity trends are very different. In NorESM2-LM (and several other models), there are significant
507 salinity trends throughout the whole water column. In NorESM2-LM, the AW salinity decreases
508 in all regions, especially after 2040, contributing to the weakening of the stratification. In the AB
509 regions, this is balanced by a stronger freshening of the surface, but in the western EB, the surface
510 is getting saltier, meaning that both the AW layer and the surface layer contribute to a weakening
511 of the density gradient. Fig. 11 shows the trend in density at each depth level over 2015–2070
512 for the two models. The combined effects of temperature and salinity yield an overall decrease in
513 density throughout the whole upper 800 m of the water column for these two models. In GFDL-
514 CM4, the profiles look similar for all four regions, with the largest decrease in the upper ocean and
515 gradually decreasing trends with depth, increasing the gradient between the upper and intermediate
516 layers. In NorESM2-LM, the profiles in the AB look similar, but in the EB regions, the (negative)
517 density trend increases with depth in the upper 200 m (red box, Fig. 11), resulting in a decreased
518 density gradient there. The density trend profiles provide a nice way to compare the hydrographic
519 changes with depth in the various regions and highlight how differently the hydrographic structure
520 is transformed in the multiple models under a similar climatic forcing. The density trend profiles
521 for all models are shown in Fig. 12.

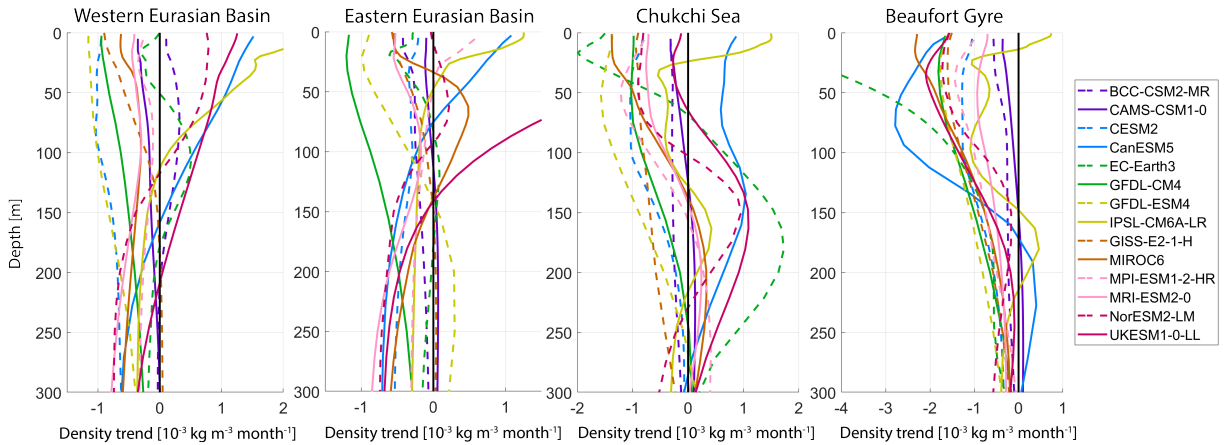
527 In the EB, most models agree on a negative density trend below 200 m, but above they diverge.
528 Here we also see large discrepancies in how quickly the density trends increase or decrease with
529 depth, thus the extent of the water column that is changed. Again, this is related to the SML depth,
530 which varies and changes differently over time (Fig. 12). In the Beaufort Gyre region, the models
531 have a very similar shape, but already in the Chukchi Sea, we see that models start to diverge, with
532 some projecting densification of the water column and some projecting a negative trend in density
533 throughout the water column. To summarize, there are many reasons why the models diverge on
534 future stratification in the EB – the divergence is partly related due to different/opposite trends
535 at the surface and partly due to a different balance between the strength of density trends at the
536 surface and at AW depth, or both.



522 FIG. 11. Monthly mean upper ocean density from GFDL-CM4 (a) and NorESM2-LM (c) from 1960 to 2100
 523 for the regions identified in Fig. 1. Linear trends are calculated for each depth level from 2015 to 2070 for
 524 GFDL-CM4 (b) and NorESM2-LM (d). Red boxes indicate the depth interval in the Western EB and Eastern EB
 525 regions where the slope of the density trend profile is opposite for the two models, resulting in opposite changes
 526 to the stratification.

541 *e. More Atlantification in the future?*

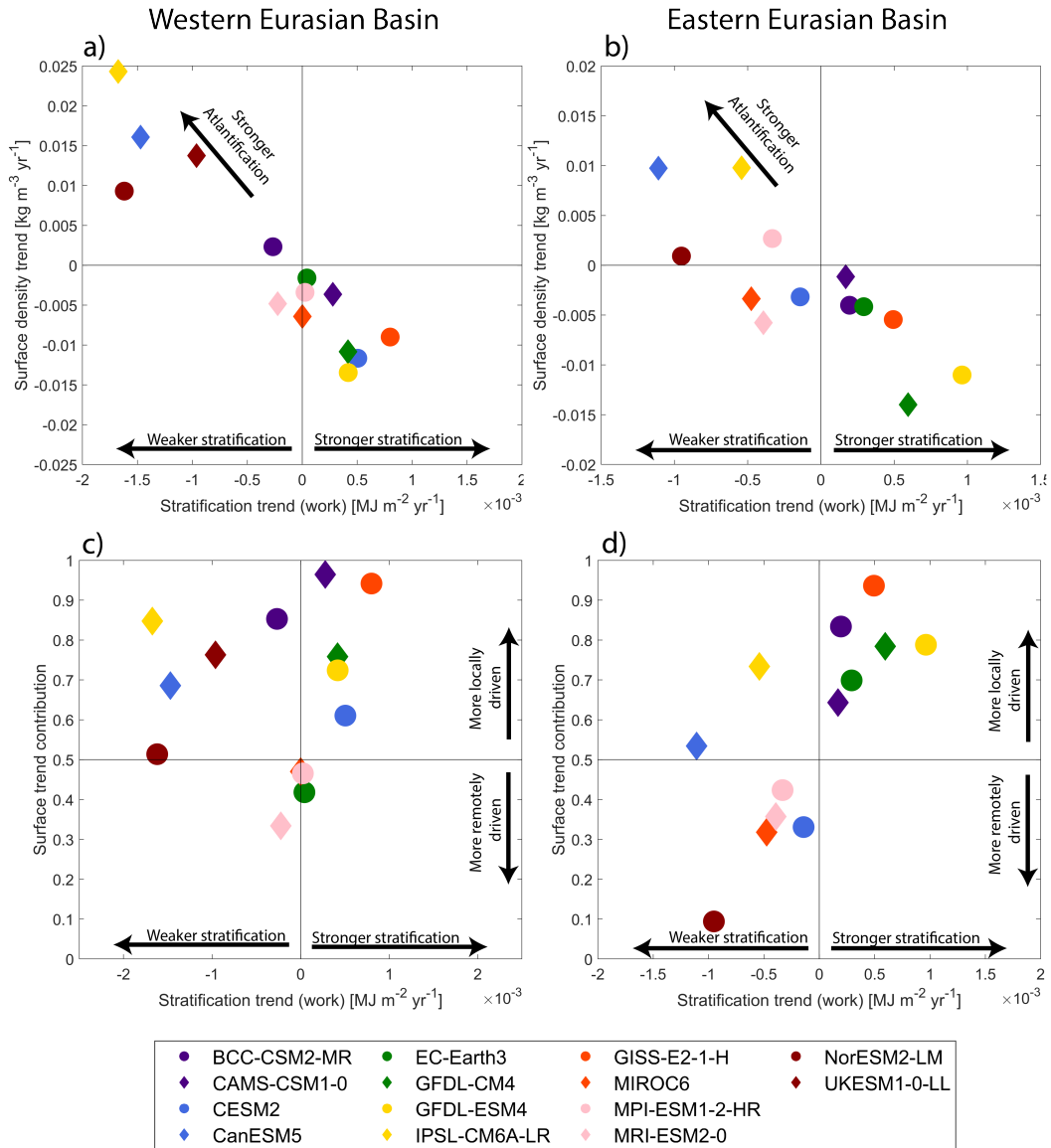
542 Under the ssp585 strong greenhouse-gas forcing scenario, there is good agreement among the
 543 models that the Arctic Ocean will continue to warm into the future with the largest warming in the
 544 AW layer and the EB. Accompanying this warming is a northward shift of ecosystems (Polyakov
 545 et al. 2020a, and references therein), a diminishing sea ice cover (Notz and SIMIP~Community



537 FIG. 12. Regional vertical profiles of the linear trend in density (similar to Fig. 11b and 11d) over the period
 538 2015–2070 from the CMIP6 models listed in Table 1. A stronger (negative) trend near the surface (~ 0–100 m)
 539 compared to intermediate depths (~ 150–300 m) results in a strengthened stratification. Note the different x-axis
 540 for each panel.

546 2020), and further changes that we can combine under the term Atlantification, as parts of the
 547 Arctic Ocean gradually become more similar to the North Atlantic. However, it is not given
 548 whether Atlantification will continue to be a metonymy for “weakening in stratification” – its
 549 primary manifestation in the Eastern EB in recent decades (Polyakov et al. 2017).

557 The top panels of Fig. 13 show the future “degree” of Atlantification (here solely defined as
 558 a weakening in stratification) for the different models in the EB. We have plotted the strength
 559 (and direction) of the upper ocean (0–50 m) density trend against the trend in stratification in the
 560 region. We observe that most models that get a denser surface layer experience a weakening in
 561 the stratification (similar to what we observe today). Models with the strongest positive trend in
 562 upper ocean density and the strongest weakening in the overall stratification thus have the strongest
 563 manifestation/degree of Atlantification. IPSL-CM6A-LR, UKESM1-0-LL (excluded from panels
 564 b) and d) because it has a surface density trend four times larger than all other models), CanESM5,
 565 and NorESM2-LM are the models with the strongest degree of future Atlantification in both the
 566 Western and Eastern EB. In contrast, GFDL-CM4, GFDL-ESM4, GISS-E2-1-H, and CESM2
 567 have the smallest degree of future Atlantification as they project a strong decrease in upper ocean
 568 density. Since the models are roughly equally divided among the two different scenarios, it is
 569 unclear whether the currently ongoing weakening of the stratification in the EB will continue or



550 FIG. 13. "Degree" of Atlantification for all models in the Western (a) and Eastern (b) Eurasian basin, plotted
 551 as the surface density trend (y-axis) against the trend in $work$ to overcome stratification (x-axis). Panels (c) and
 552 (d) show the relative size of surface density trends v.s. AW density trends in the Western and Eastern Eurasian
 553 basin (y-axis) are plotted against the trend in $work$ to overcome stratification (x-axis). $y = 0.5$ means equally
 554 strong density trends in the surface compared to the AW layer, and $y > 0.5$ means larger trends in the surface.
 555 Note the different axis limits between panels. UKESM1-0-LL is excluded from panels b) and d) because it has a
 556 surface density trend four times larger than all other models.

570 not. Following Heuzé et al. (2022) and Khosravi et al. (2022), there is no clear evidence of certain
571 models being significantly better at accurately reproducing the Arctic Ocean hydrography and
572 circulation, and we can therefore not favor certain models or either of the scenarios. There is also
573 no clear relationship between models with higher or lower resolution. To gain confidence in a
574 future scenario, we need first to improve the models. As shown in our companion paper, Heuzé
575 et al. (2022), these improvements could focus on ventilation and dense water overflows. There are
576 also large biases in AW flow speed and patterns, and most CMIP6 models show a strong decoupling
577 between the upper layers and the rest of the deep Arctic not consistent with observations.

578 The model biases and different behaviors in the EB are probably not solely related to biases
579 and processes within the Arctic, as the changes are both locally and remotely driven. We can
580 assume that the changes in the upper ocean are primarily driven from within the Arctic and that
581 the changes in the AW layer are driven partly from within the Arctic and partly from outside the
582 Arctic Ocean. As this balance between local and remote forcing is likely to differ among models,
583 it could also contribute to explaining the model divergence on stratification in the EB. In Figs. 13c
584 and 13d, we present the relative size of upper ocean v.s. AW density changes in the Western and
585 Eastern EB. In the Western EB, most models have stronger trends in the upper ocean than the AW
586 layer (values larger than 0.5). There is no evident relationship between the balance and the sign
587 of the stratification trend. In the Eastern EB, however, there appears to be a relationship ($r=0.71$)
588 between the degree of local forcing and the change in stratification (Fig. 13d): models that have a
589 larger surface density change overall have an increase in stratification too. The opposite is also true:
590 weaker stratification goes with a small surface density change. This means that in the future, the
591 upper ocean density trends generally dominate over the trends in the AW. However, in the Eastern
592 EB, the density trends are of more comparable strength, and the balance between these two is thus
593 more important here.

594 **4. Discussion and conclusions**

595 This study quantified recent and future trends in upper Arctic Ocean stratification, temperature,
596 and salinity in an ensemble of 14 CMIP6 models and compared these to a unique dataset of
597 hydrographic observations dating back to 1970. In agreement with observations (e.g. Polyakov
598 et al. 2020a), the models simulate a freshening and warming of the upper Amerasian basin (AB) and

599 large parts of the Eurasian Basin (EB) over the period 1970–2014. These changes are associated
600 with a general strengthening of the stratification, although there is a large spread among the
601 simulated trends and mean stratifications. Only two out of the 14 models simulate a weakening
602 of the stratification in the Eastern EB that is comparable to observations. However, all models
603 indicate different trends in stratification in the AB and EB, and these regional differences endure
604 well into the twenty-first century.

605 Because of these temperature, salinity, and stratification biases in CMIP models, simulating
606 and defining the halocline in models is challenging, especially when studying it in a suite of
607 models under a climate change scenario. To compare and evaluate simulated Arctic stratification
608 meaningfully, we, therefore, proposed a new indicator of stratification, termed “*work*” to overcome
609 stratification (ΔPE). This is an integral of the potential energy needed to fully mix the water
610 column from the surface down to 300 m depth. Typical Arctic Ocean values are about 0.1 MJ m^{-2} ,
611 but the Beaufort Gyre and the Chukchi Sea have twice as strong stratification. Temporal change
612 and regional contrasts observed by more traditional stratification definitions (e.g. Polyakov et al.
613 2020a) are captured well by this new parameter, whose definition is not sensitive to model biases.

614 There is a reassuring across-model agreement within the Beaufort Gyre and the Chukchi Sea for
615 near-surface stratification. Here the upper ocean layer will become fresher (on average 0.18 psu
616 decade^{-1}), warmer (on average $0.35 \text{ }^\circ\text{C decade}^{-1}$) and more stratified in the future (on average 1.1
617 $\times 10^{-4} \text{ MJ m}^{-2} \text{ decade}^{-1}$), but there is a large spread in the magnitude. There is also simulated
618 future warming ($0.24 \text{ }^\circ\text{C decade}^{-1}$) and freshening ($-0.03 \text{ psu decade}^{-1}$) occurring further down
619 in the Atlantic Water (AW) layer. The entire water column is therefore getting less dense, but
620 the surface freshening is so strong that the stratification is overall increasing in these regions.
621 We did not examine the detailed causes of the future surface freshening but hold it as likely that
622 both redistribution and local melting of sea ice, increased river runoff, increased glacial melt, and
623 increased freshwater inflow through Bering Strait will all contribute significantly – as they do today
624 (Haine et al. 2015; Haine 2020; Solomon et al. 2021). Throughout the upper Arctic Ocean, density
625 trends are dominated by changes in salinity, but at intermediate depth, temperature and salinity
626 changes contribute equally to the density trends.

627 There is a divergence between the models regarding future stratification in both the Eastern and
628 Western EB. Approximately half of the models project a strengthening of stratification here, and

629 the other half project the opposite. The divergence is caused by opposing trends in upper ocean
630 temperature and salinity. Furthermore, we discuss how the differences in stratification are related
631 to different balances between trends in the upper ocean and trends at intermediate depths. Across
632 the suite of models, there is a warming of the EB AW layer, but it varies between 0-7°C towards the
633 end of the century. A majority of the models also project a freshening of the EB AW layer (0-0.9
634 psu), starting approximately in the 2050s. The AW warming and freshening result in a reduced
635 density at intermediate depths, weakening the stratification. In about half of the models, these
636 changes are counterbalanced by an upper-ocean freshening resulting in a strengthened stratification
637 also in the EB. However, in some models, parts of the EB upper ocean experience a salinification,
638 or the AW density change dominates (or both), aiding to an overall weakened stratification. It is
639 difficult to judge which of the two stratification scenarios is the most likely.

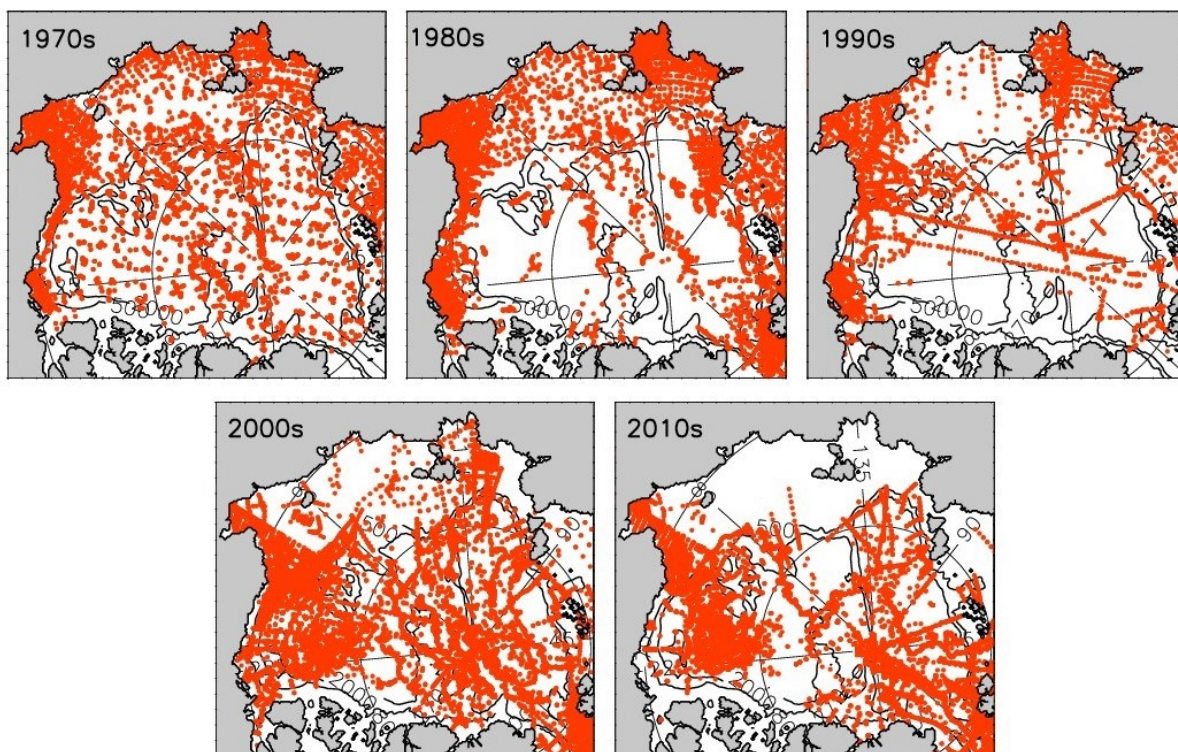
640 In summary, observations and simulations agree that the Arctic Ocean is becoming warmer and
641 that there is ongoing freshening in the AB. The simulations also agree that the observed weakening
642 of the stratification in the EB does not spread eastward into the AB. The warming is unsurprising
643 on a globally warming planet, and the future warming of the AW layer is most pronounced. In that
644 regard, it is consistent with using the term Atlantification – as these waters are becoming more
645 similar to those further south. However, it is unclear whether Atlantification will continue to be
646 analogous to a weakening in stratification. Of the models we analyzed, half of the models predicted
647 a strengthening of the EB stratification. This is not what is currently associated with Atlantification.
648 Further work is thus required before we can have more confidence in the future development of the
649 EB. First, we need to improve the model's capability to simulate Arctic hydrography. Particular
650 emphasis should be on the representation of AW circulation, ventilation, and the connections
651 between the shelves and the deep basins (Heuzé et al. 2022). Additionally, there is an urgent need
652 for more multi-scale (in time and space) observational campaigns, such as the recent MOSAiC
653 expedition (Rabe et al. 2022), that simultaneously provide in-situ data of all the components of the
654 Arctic climate system. Such campaigns result in a better understanding of specific processes and
655 their interaction, which then can be used to improve their representation in the models. Long-term
656 mooring deployments in the Central Arctic are also needed to understand the variability at various
657 timescales.

658 Our study highlights the importance of a multi-model approach for studies of the future Arctic
659 Ocean. Given the relatively large biases and opposite trends, relying on a single or just a few
660 model systems is insufficient and may result in misleading conclusions. However, it is important to
661 analyze and interpret the models individually, not as a multi-model mean. Our results clearly show
662 that averaging (opposite) model trends and properties will yield results that seem credible but are
663 completely nonphysical. This is particularly important for profiles - as water masses are distributed
664 differently in the vertical, and the same processes, therefore, have an effect at different depths.
665 Thus, an important takeaway from this study is that we strongly discourage using multi-model
666 averages to investigate trends in Arctic hydrography. Also, many ensembles from a single model
667 system may skew the results towards specific model biases created by physical or thermodynamical
668 deficiencies. Clearly, studies of the Arctic Ocean should be based on and validated by observations
669 due to the inherent large local uncertainty of the models.

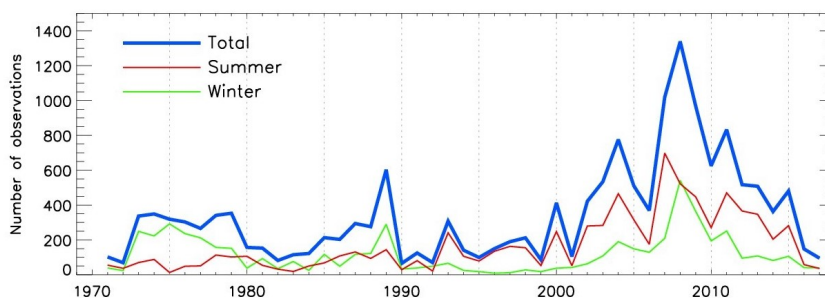
670 *Acknowledgments.* Morven Muilwijk received funding for this work from the European Union's
671 Horizon 2020 research and innovation programme under grant agreement No 101003826 via
672 project CRiceS (Climate Relevant interactions and feedbacks: the key role of sea ice and Snow
673 in the polar and global climate system) and from the University of Bergen, Bjerknes Center for
674 Climate Research. Aleksi Nummelin received funding for this work from Research Council of
675 Norway project KeyClim (295046). Igor V. Polyakov acknowledges support from the United States
676 NSF grants (AON-1724523, AON-1947162) and ONR grant (N00014-21-1-2577). Céline Heuzé
677 received funding for this work from Vetenskapsrådet under grant agreement 2018-03859. Support
678 for Hannah Zanowski was provided by the Office of the Vice Chancellor for Research and Graduate
679 Education at the University of Wisconsin–Madison with funding from the Wisconsin Alumni
680 Research Foundation. The authors acknowledge the World Climate Research Programme, which,
681 through its Working Group on Coupled Modelling, coordinated and promoted CMIP6. The authors
682 also thank the various modeling groups for producing and making their model output available,
683 the Earth Grid System Federation (ESGF) for archiving and providing access, and the multiple
684 funding agencies that support CMIP6 and ESGF. Computing and storage resources were provided
685 by Sigma2 - the National Infrastructure for High-Performance Computing and Data Storage in
686 Norway, and the authors would like to thank Michael Schulz, Yanchun He, and Richard Davy
687 for coordinating the local storage of CMIP6 data and Anais Bretones for support with the data
688 download. Finally, the authors would also like to thank those who went to sea and collected
689 valuable observations in harsh Arctic conditions over the last century.

690 *Data availability statement.* CMIP6 data are freely available via the Earth Grid System Federation.
691 For the analysis presented here, we used the Geophysical Fluid Dynamics Laboratory (GFDL) node:
692 <https://esgdata.gfdl.noaa.gov/search/cmip6-gfdl/> and the Lawrence Livermore Na-
693 tional Laboratory node: <https://esgf-node.llnl.gov/projects/cmip6/>. 1981–2017 Arc-
694 tic Ocean CTD data are available online via Pangaea Data Publisher.

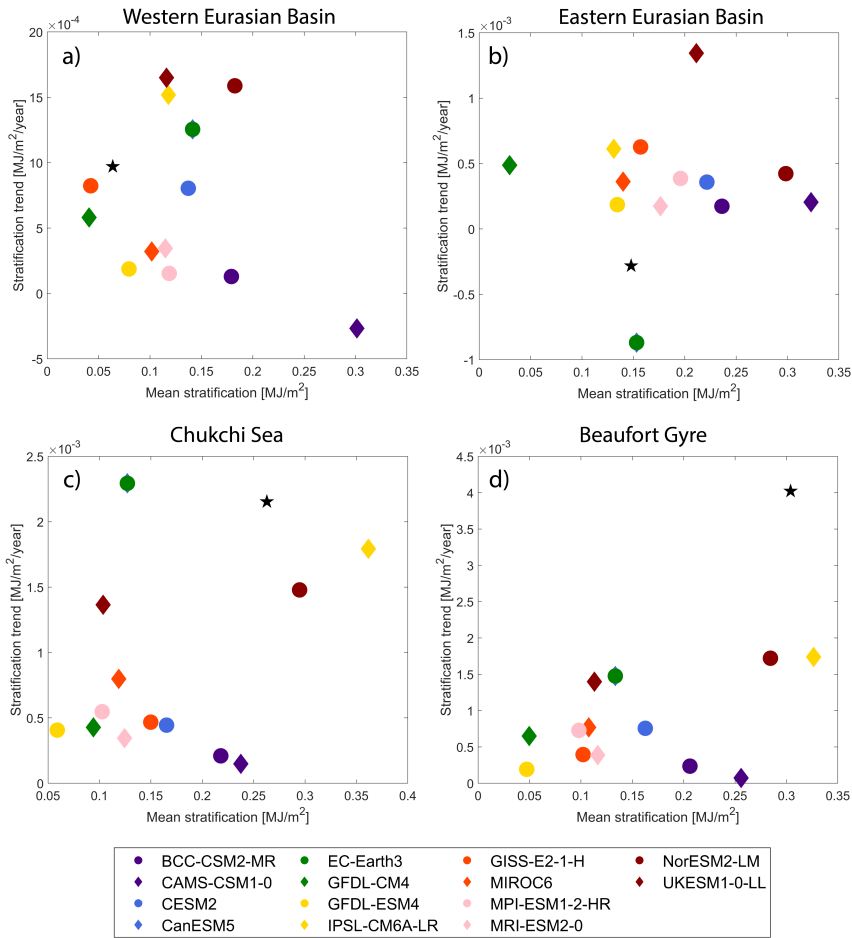
695 APPENDIX



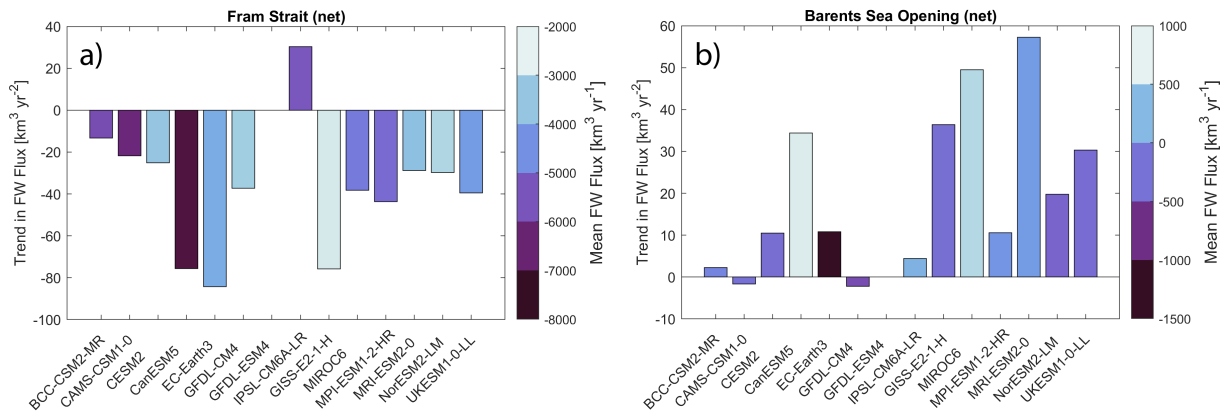
696 FIG. A1. Temporal and spatial data coverage for each of the decades in the observational data set used in this
 697 study.



698 FIG. A2. Number of hydrographic observations per season for the Eurasian basin and Amerasian basin regions
 699 combined.



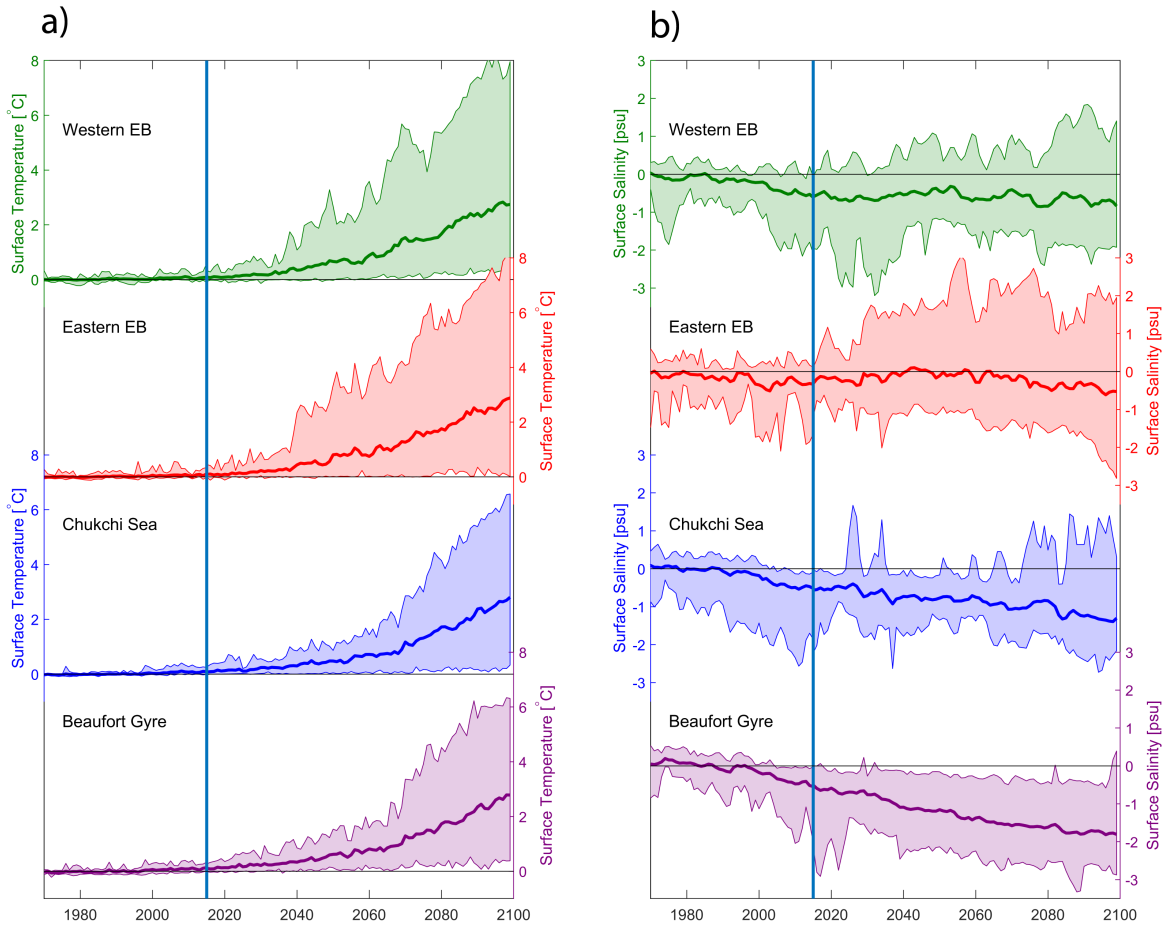
700 FIG. A3. Simulated mean *work* to overcome stratification versus trends in *work* to overcome stratification for
 701 each of the CMIP6 models listed in Table 1 over 1970–2014. Black stars indicate the observed values.



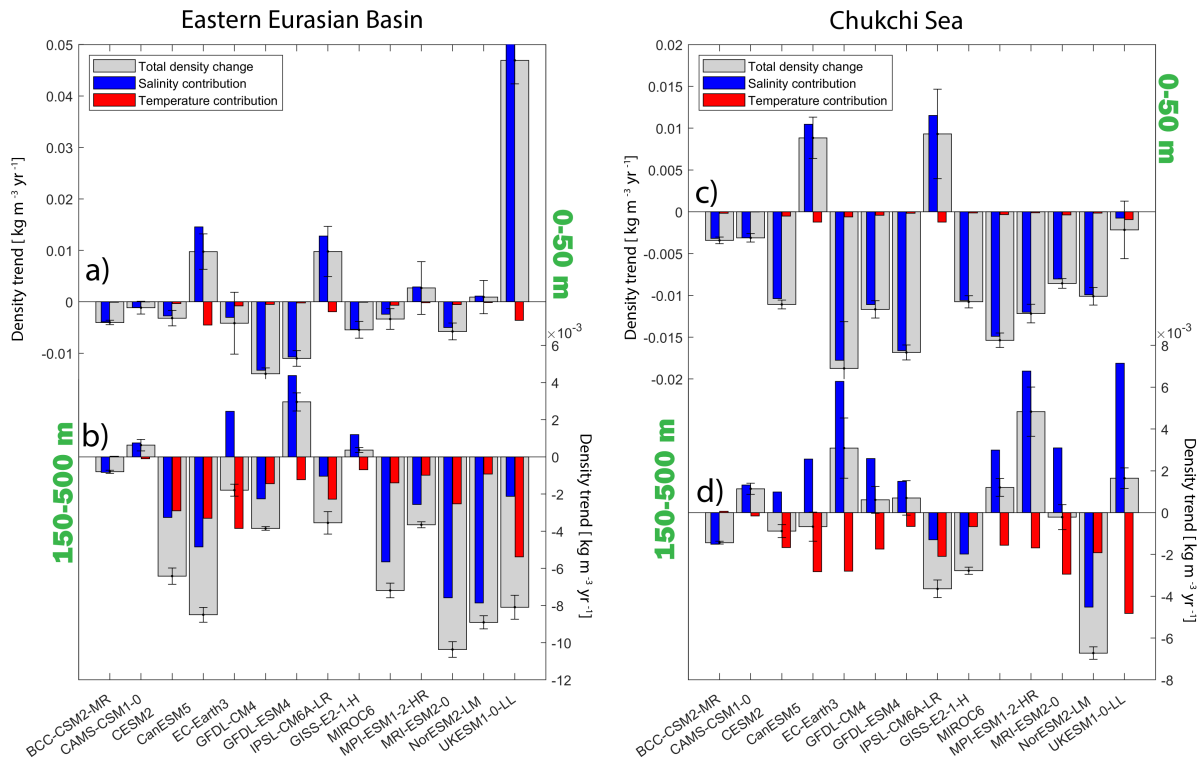
702 FIG. A4. Trends in net liquid freshwater flux ($\text{km}^3 \text{yr}^{-2}$) from 2015–2070 at a) Fram Strait and b) the Barents
 703 Sea Opening for the ssp585 future scenario. Color shading indicates the mean net liquid freshwater flux for each
 704 model over the same time period. Positive direction is northward (Fram Strait experiences a net southward flux
 705 of freshwater). Velocity data from GFDL-ESM4 was not available and therefore no fluxes could be calculated
 706 for this model.

715 TABLE A1. Future upper ocean (0–50 m) temperature and salinity trends for each of the CMIP6 models
 716 (forcing scenario ssp585) over 2015–2070. Values are given in $^{\circ}\text{C} \text{decade}^{-1}$ and $\text{psu} \text{decade}^{-1}$. Statistically
 717 non-significant trends ($p \geq 0.05$) are shown in italic.

	Western EB		Eastern EB		Chukchi Sea		Beaufort Gyre	
	θ	S	θ	S	θ	S	θ	S
BCC-CSM2-MR	.044 ± .006	.030 ± .007	.049 ± .007	-.048 ± .005	.083 ± .011	-.039 ± .005	.082 ± .017	-.074 ± .005
CAMS-CSM1-0	.018 ± .004	-.045 ± .021	.006 ± .003	-.014 ± .016	.012 ± .003	-.038 ± .006	.023 ± .008	-.043 ± .005
CESM2	.124 ± .009	-.139 ± .007	.134 ± .014	-.034 ± .019	.183 ± .017	-.129 ± .007	.189 ± .017	-.163 ± .007
CanESM5	.823 ± .044	.252 ± .037	.857 ± .039	.172 ± .042	.374 ± .018	.125 ± .031	.381 ± .019	-.307 ± .016
EC-Earth3	.191 ± .021	-.021 ± .053	.166 ± .022	-.052 ± .067	.176 ± .022	-.227 ± .069	.258 ± .013	-.703 ± .047
GFDL-CM4	.138 ± .012	-.127 ± .011	.150 ± .015	-.167 ± .014	.153 ± .013	-.139 ± .013	.175 ± .016	-.252 ± .009
GFDL-ESM4	.067 ± .009	-.163 ± .015	.087 ± .012	-.136 ± .018	.070 ± .008	-.209 ± .011	.077 ± .009	-.251 ± .009
IPSL-CM6A-LR	.393 ± .035	.279 ± .053	.299 ± .029	.099 ± .051	.258 ± .021	.060 ± .071	.238 ± .022	-.064 ± .066
GISS-E2-1-H	.022 ± .003	-.106 ± .017	.043 ± .004	-.063 ± .019	.061 ± .008	-.132 ± .009	.081 ± .007	-.232 ± .009
MIROC6	.271 ± .027	-.064 ± .015	.209 ± .023	-.022 ± .025	.133 ± .012	-.182 ± .011	.131 ± .016	-.319 ± .012
MPI-ESM1-2-HR	.071 ± .009	-.040 ± .026	.083 ± .009	.036 ± .063	.061 ± .008	-.149 ± .014	.093 ± .011	-.186 ± .009
MRI-ESM2-0	.197 ± .020	-.049 ± .013	.148 ± .023	-.062 ± .020	.104 ± .020	-.102 ± .007	.230 ± .022	-.110 ± .010
NorESM2-LM	.032 ± .006	.116 ± .026	.066 ± .009	.017 ± .040	.071 ± .009	-.125 ± .013	.103 ± .012	-.246 ± .014
UKESM1-0-LL	.491 ± .030	.190 ± .039	.714 ± .056	.583 ± .054	.272 ± .014	-.019 ± .043	.320 ± .017	-.269 ± .024



707 FIG. A5. Regional time series of normalized (reduced to anomalies relative to 1970-2014 model mean) upper
 708 ocean temperature (a) and upper ocean salinity (b) from the CMIP6 models listed in Table 1. Thick lines represent
 709 the multimodel mean and envelopes shows the minimum and maximum of the model spread per time-step. The
 710 upper ocean properties are calculated as the vertical average between 0–50 m.



711 FIG. A6. Trends in density in the upper ocean (a) and c) and Atlantic Water layer (b) and d) for the Eastern
 712 Eurasian basin (left) and the Chukchi Sea region (right) for each of the CMIP6 models listed in Table 1. Red and
 713 blue bars denote the relative contributions of temperature and salinity trends to the total density trends (fat grey
 714 bars). Positive values mean increased density and negative values mean decreased density.

718 **References**

- 719 Aagaard, K., L. Coachman, and E. Carmack, 1981: On the halocline of the Arctic Ocean. *Deep*
720 *Sea Research Part A. Oceanographic Research Papers*, **28 (6)**, 529–545, [https://doi.org/10.1016/](https://doi.org/10.1016/0198-0149(81)90115-1)
721 [0198-0149\(81\)90115-1](https://doi.org/10.1016/0198-0149(81)90115-1).
- 722 Adcroft, A., and Coauthors, 2019: The GFDL global ocean and sea ice model OM4. 0: Model
723 description and simulation features. *Journal of Advances in Modeling Earth Systems*, **11 (10)**,
724 3167–3211, <https://doi.org/10.1029/2019MS001726>.
- 725 Amante, C., and B. W. Eakins, 2009: ETOPO1 Global Relief Model converted to PanMap layer
726 format. *NOAA-National Geophysical Data Center, PANGAEA*.
- 727 Årthun, M., and T. Eldevik, 2016: On anomalous ocean heat transport toward the Arctic and
728 associated climate predictability. *Journal of Climate*, **29 (2)**, 689–704, [https://doi.org/10.1175/](https://doi.org/10.1175/JCLI-D-15-0448.1)
729 [JCLI-D-15-0448.1](https://doi.org/10.1175/JCLI-D-15-0448.1).
- 730 Årthun, M., T. Eldevik, L. H. Smedsrud, O. Skagseth, and R. B. Ingvaldsen, 2012: Quantifying
731 the Influence of Atlantic Heat on Barents Sea Ice Variability and Retreat. *Journal of Climate*,
732 **25 (13)**, 4736–4743, <https://doi.org/10.1175/JCLI-D-11-00466.1>.
- 733 Årthun, M., I. H. Onarheim, J. Dörr, and T. Eldevik, 2021: The Seasonal and Regional Transition
734 to an Ice-Free Arctic. *Geophysical Research Letters*, **48 (1)**, e2020GL090825, [https://doi.org/](https://doi.org/10.1029/2020GL090825)
735 [10.1029/2020GL090825](https://doi.org/10.1029/2020GL090825).
- 736 Bluhm, B., K. Kosobokova, and E. Carmack, 2015: A tale of two basins: An integrated physical
737 and biological perspective of the deep Arctic Ocean. *Progress in Oceanography*, **139**, 89–121,
738 <https://doi.org/10.1016/j.pocean.2015.07.011>.
- 739 Bluhm, B. A., and Coauthors, 2020: The Pan-Arctic Continental Slope: Sharp Gradients of
740 Physical Processes Affect Pelagic and Benthic Ecosystems. *Frontiers in Marine Science*, **7**,
741 544–586, <https://doi.org/10.3389/fmars.2020.544386>.
- 742 Bourgain, P., and J. Gascard, 2011: The Arctic Ocean halocline and its interannual variability from
743 1997 to 2008. *Deep Sea Research Part I: Oceanographic Research Papers*, **58 (7)**, 745–756,
744 <https://doi.org/10.1016/j.dsr.2011.05.001>.

- 745 Carmack, E., and Coauthors, 2015: Towards Quantifying the Increasing Role of Oceanic Heat in
746 Sea Ice Loss in the New Arctic. *Bulletin of the American Meteorological Society*, **96 (12)**, 2079–
747 2105, <https://doi.org/10.1175/BAMS-D-13-00177.1>, URL [http://journals.ametsoc.org/doi/abs/
748 10.1175/BAMS-D-13-00177.1](http://journals.ametsoc.org/doi/abs/10.1175/BAMS-D-13-00177.1).
- 749 Carmack, E. C., 2007: The alpha/beta ocean distinction: A perspective on freshwater fluxes,
750 convection, nutrients and productivity in high-latitude seas. *Deep Sea Research Part II: Topical
751 Studies in Oceanography*, **54 (23-26)**, 2578–2598, <https://doi.org/10.1016/j.dsr2.2007.08.018>.
- 752 Carmack, E. C., and Coauthors, 2016: Freshwater and its role in the Arctic Marine System:
753 Sources, disposition, storage, export, and physical and biogeochemical consequences in the
754 Arctic and global oceans. *Journal of Geophysical Research G: Biogeosciences*, **121 (3)**, 675–
755 717, <https://doi.org/10.1002/2015JG003140>.
- 756 Cohen, J., and Coauthors, 2020: Divergent consensus on Arctic amplification influence on
757 midlatitude severe winter weather. *Nature Climate Change*, **10 (1)**, 20–29, [https://doi.org/10.
758 1038/s41558-019-0662-y](https://doi.org/10.1038/s41558-019-0662-y).
- 759 Cornish, S. B., Y. Kostov, H. L. Johnson, and C. Lique, 2020: Response of Arctic freshwater
760 to the Arctic Oscillation in coupled climate models. *Journal of Climate*, **33 (7)**, 2533–2555,
761 <https://doi.org/10.1175/JCLI-D-19-0685.1>.
- 762 Danabasoglu, G., and Coauthors, 2020: The Community Earth System Model Version 2 (CESM2).
763 *Journal of Advances in Modeling Earth Systems*, **12 (2)**, e2019MS001916, [https://doi.org/
764 10.1029/2019MS001916](https://doi.org/10.1029/2019MS001916).
- 765 Davy, R., and S. Outten, 2020: The Arctic Surface Climate in CMIP6: Status and De-
766 velopments since CMIP5. *Journal of Climate*, **33 (18)**, 8047–8068, [https://doi.org/10.1175/
767 JCLI-D-19-0990.1](https://doi.org/10.1175/JCLI-D-19-0990.1).
- 768 Döscher, R., and Coauthors, 2021: The EC-earth3 Earth system model for the climate model
769 intercomparison project 6. *Geoscientific Model Development Discussions*, 1–90, [https://doi.org/
770 10.5194/gmd-2020-446](https://doi.org/10.5194/gmd-2020-446).

771 Dunne, J. P., and Coauthors, 2020: The GFDL Earth System Model Version 4.1 (GFDL-ESM
772 4.1): Overall Coupled Model Description and Simulation Characteristics. *Journal of Advances*
773 *in Modeling Earth Systems*, **12** (11), e2019MS002 015, <https://doi.org/10.1029/2019MS002015>.

774 Eyring, V., S. Bony, G. A. Meehl, C. A. Senior, B. Stevens, R. J. Stouffer, and K. E. Taylor,
775 2016: Overview of the Coupled Model Intercomparison Project Phase 6 (CMIP6) experimental
776 design and organization. *Geoscientific Model Development*, **9** (5), 1937–1958, [https://doi.org/](https://doi.org/10.5194/gmd-9-1937-2016)
777 [10.5194/gmd-9-1937-2016](https://doi.org/10.5194/gmd-9-1937-2016).

778 Giles, K. a., S. W. Laxon, A. L. Ridout, D. J. Wingham, and S. Bacon, 2012: Western Arctic Ocean
779 freshwater storage increased by wind-driven spin-up of the Beaufort Gyre. *Nature Geoscience*,
780 **5** (3), 194–197, <https://doi.org/10.1038/ngeo1379>.

781 Gorshkov, S. G., 1980: Atlas of Oceans. Arctic Ocean. *Minist. of Def. of the USSR, Moscow*.

782 Haine, T. W., and Coauthors, 2015: Arctic freshwater export: Status, mechanisms, and prospects.
783 *Global and Planetary Change*, **125**, 13–35, <https://doi.org/10.1016/j.gloplacha.2014.11.013>.

784 Haine, T. W. N., 2020: Arctic Ocean Freshening Linked to Anthropogenic Climate Change:
785 All Hands on Deck. *Geophysical Research Letters*, **47** (22), e2020GL090 678, [https://doi.org/](https://doi.org/10.1029/2020GL090678)
786 [10.1029/2020GL090678](https://doi.org/10.1029/2020GL090678).

787 Held, I. M., and B. J. Soden, 2006: Robust responses of the hydrological cycle to global warming.
788 *Journal of climate*, **19** (21), 5686–5699, <https://doi.org/10.1175/JCLI3990.1>.

789 Heuzé, C., 2021: Antarctic Bottom Water and North Atlantic Deep Water in CMIP6 models. *Ocean*
790 *Science*, **17** (1), 59–90, <https://doi.org/10.5194/os-17-59-2021>.

791 Heuzé, C., H. Zanowski, S. Karam, and M. Muilwijk, 2022: The deep Arctic Ocean and Fram
792 Strait in CMIP6 models. *Submitted to Journal of Climate*.

793 Holland, M. M., J. Finnis, A. P. Barrett, and M. C. Serreze, 2007: Projected changes in Arctic
794 Ocean freshwater budgets. *Journal of Geophysical Research: Biogeosciences*, **112** (G4), n/a–n/a,
795 <https://doi.org/10.1029/2006JG000354>.

- 796 Holmes, R. M., and Coauthors, 2012: Seasonal and Annual Fluxes of Nutrients and Organic
797 Matter from Large Rivers to the Arctic Ocean and Surrounding Seas. *Estuaries and Coasts*,
798 **35** (2), 369–382, <https://doi.org/10.1007/s12237-011-9386-6>.
- 799 Ilicak, M., and Coauthors, 2016: An assessment of the Arctic Ocean in a suite of interannual CORE-
800 II simulations. Part III: Hydrography and fluxes. *Ocean Modelling*, **100**, 141–161, <https://doi.org/10.1016/j.ocemod.2016.02.004>.
- 802 IPCC, 2021: *Climate Change 2021: The Physical Science Basis. Contribution of Working Group*
803 *I to the Sixth Assessment Report of the Intergovernmental Panel on Climate Change*. Cambridge
804 University Press.
- 805 Jahn, A., and R. Laiho, 2020: Forced Changes in the Arctic Freshwater Budget Emerge in the
806 Early 21st Century. *Geophysical Research Letters*, **47** (15), e2020GL088854, <https://doi.org/10.1029/2020GL088854>.
- 808 Kattsov, V. M., J. E. Walsh, W. L. Chapman, V. A. Govorkova, T. V. Pavlova, and X. Zhang,
809 2007: Simulation and Projection of Arctic Freshwater Budget Components by the IPCC AR4
810 Global Climate Models. *Journal of Hydrometeorology*, **8** (3), 571–589, [https://doi.org/10.1175/](https://doi.org/10.1175/JHM575.1)
811 [JHM575.1](https://doi.org/10.1175/JHM575.1).
- 812 Kelley, M., and Coauthors, 2020: GISS-E2.1: Configurations and Climatology. *Journal of*
813 *Advances in Modeling Earth Systems*, **12** (8), e2019MS002025, [https://doi.org/10.1029/](https://doi.org/10.1029/2019MS002025)
814 [2019MS002025](https://doi.org/10.1029/2019MS002025).
- 815 Khosravi, N., Q. Wang, N. Koldunov, C. Hinrichs, T. Semmler, S. Danilov, and T. Jung, 2022: The
816 Arctic Ocean in CMIP6 Models: Biases and Projected Changes in Temperature and Salinity.
817 *Earth's Future*, **10** (2), e2021EF002282, <https://doi.org/10.1029/2021EF002282>.
- 818 Li, G., L. Cheng, J. Zhu, K. E. Trenberth, M. E. Mann, and J. P. Abraham, 2020: Increasing
819 ocean stratification over the past half-century. *Nature Climate Change*, **10** (12), 1116–1123,
820 <https://doi.org/10.1038/s41558-020-00918-2>.
- 821 Lurton, T., and Coauthors, 2020: Implementation of the CMIP6 Forcing Data in the IPSL-
822 CM6A-LR Model. *Journal of Advances in Modeling Earth Systems*, **12** (4), e2019MS001940,
823 <https://doi.org/10.1029/2019MS001940>.

- 824 McDougall, T. J., and P. M. Barker, 2011: *Getting started with TEOS-10 and the Gibbs Seawater*
825 *(GSW) Oceanographic Toolbox*. SCOR/IAPSO, 28 pp., URL www.TEOS-10.org.
- 826 Metzner, E. P., M. Salzmann, and R. Gerdes, 2020: Arctic Ocean Surface Energy Flux and the Cold
827 Halocline in Future Climate Projections. *Journal of Geophysical Research: Oceans*, **125** (2),
828 e2019JC015 554, <https://doi.org/10.1029/2019JC015554>.
- 829 Muilwijk, M., and Coauthors, 2019: Arctic Ocean Response to Greenland Sea Wind Anomalies in
830 a Suite of Model Simulations. *Journal of Geophysical Research: Oceans*, **124** (8), 6286–6322,
831 <https://doi.org/10.1029/2019JC015101>.
- 832 Müller, W. A., and Coauthors, 2018: A Higher-resolution Version of the Max Planck Institute
833 Earth System Model (MPI-ESM1.2-HR). *Journal of Advances in Modeling Earth Systems*,
834 **10** (7), 1383–1413, <https://doi.org/10.1029/2017MS001217>.
- 835 Nansen, F., 1902: *The oceanography of the north polar basin*, Vol. 3. Longmans, Green, and
836 Company.
- 837 Nguyen, a. T., D. Menemenlis, and R. Kwok, 2009: Improved modeling of the Arctic halocline with
838 a subgrid-scale brine rejection parameterization. *Journal of Geophysical Research*, **114** (C11),
839 C11 014, <https://doi.org/10.1029/2008JC005121>.
- 840 Notz, D., and SIMIP~Community, 2020: Arctic Sea Ice in CMIP6. *Geophysical Research Letters*,
841 **47** (10), e2019GL086 749, <https://doi.org/10.1029/2019GL086749>.
- 842 Nummelin, A., M. Ilicak, C. Li, and L. H. Smedsrud, 2016: Consequences of future increased
843 Arctic runoff on Arctic Ocean stratification, circulation, and sea ice cover. *Journal of Geophysical*
844 *Research: Oceans*, **121** (1), 617–637, <https://doi.org/10.1002/2015JC011156>.
- 845 Nummelin, A., C. Li, and L. H. Smedsrud, 2015: Response of Arctic Ocean stratification to
846 changing river runoff in a column model. *Journal of Geophysical Research: Oceans*, **120** (4),
847 2655–2675, <https://doi.org/10.1002/2014JC010571>.
- 848 Onarheim, I. H., T. Eldevik, M. Årthun, R. B. Ingvaldsen, and L. H. Smedsrud, 2015: Skill-
849 ful prediction of Barents Sea ice cover. *Geophysical Research Letters*, **42** (13), 5364–5371,
850 <https://doi.org/10.1002/2015GL064359>.

851 Peralta-Ferriz, C., and R. A. Woodgate, 2015: Seasonal and interannual variability of pan-Arctic
852 surface mixed layer properties from 1979 to 2012 from hydrographic data, and the dominance of
853 stratification for multiyear mixed layer depth shoaling. *Progress in Oceanography*, **134**, 19–53,
854 <https://doi.org/10.1016/j.pocean.2014.12.005>.

855 Peterson, B. J., R. M. Holmes, J. W. McClelland, C. J. V"{}r"{}smarty, R. B. Lammers, A. I.
856 Shiklomanov, I. A. Shiklomanov, and S. Rahmstorf, 2002: Increasing River Discharge to the
857 Arctic Ocean. *Science*, **298 (5601)**, 2171–2173, <https://doi.org/10.1126/science.1077445>.

858 Polyakov, I. V., A. V. Pnyushkov, and E. C. Carmack, 2018: Stability of the arctic halocline: A
859 new indicator of arctic climate change. *Environmental Research Letters*, **13 (12)**, <https://doi.org/10.1088/1748-9326/aac1e>.

861 Polyakov, I. V., and Coauthors, 2017: Greater role for Atlantic inflows on sea-ice loss in the
862 Eurasian Basin of the Arctic Ocean. *Science*, **291 (April)**, 285–291, <https://doi.org/10.1126/science.aai8204>.

864 Polyakov, I. V., and Coauthors, 2020a: Borealization of the Arctic Ocean in Response to Anomalous
865 Advection From Sub-Arctic Seas. *Frontiers in Marine Science*, **7**, <https://doi.org/10.3389/fmars.2020.00491>.

867 Polyakov, I. V., and Coauthors, 2020b: Weakening of Cold Halocline Layer Exposes Sea Ice
868 to Oceanic Heat in the Eastern Arctic Ocean. *Journal of Climate*, **33 (18)**, 8107–8123,
869 <https://doi.org/10.1175/JCLI-D-19-0976.1>.

870 Proshutinsky, a., 2002: The role of the Beaufort Gyre in Arctic climate variability: Seasonal to
871 decadal climate scales. *Geophysical Research Letters*, **29 (23)**, 2100, <https://doi.org/10.1029/2002GL015847>.

873 Proshutinsky, A., and Coauthors, 2009: Beaufort Gyre freshwater reservoir: State and variability
874 from observations. *Journal of Geophysical Research*, **114**, C00A10, <https://doi.org/10.1029/2008JC005104>.

876 Proshutinsky, A., and Coauthors, 2019: Analysis of the Beaufort Gyre freshwater content in
877 2003–2018. *Journal of Geophysical Research: Oceans*, **124 (12)**, 9658–9689, <https://doi.org/10.1029/2019JC015281>.

878

879 Rabe, B., and Coauthors, 2011: An assessment of Arctic Ocean freshwater content changes from
880 the 1990s to the 2006–2008 period. *Deep Sea Research Part I: Oceanographic Research Papers*,
881 **58 (2)**, 173–185, <https://doi.org/10.1016/j.dsr.2010.12.002>.

882 Rabe, B., and Coauthors, 2014: Arctic Ocean basin liquid freshwater storage trend 1992–2012.
883 *Geophysical Research Letters*, **41 (3)**, 961–968, <https://doi.org/10.1002/2013GL058121>.

884 Rabe, B., and Coauthors, 2022: Overview of the MOSAiC expedition: Physical oceanography.
885 *Elementa: Science of the Anthropocene*, **10 (1)**, 62, [https://doi.org/10.1525/elementa.2021.](https://doi.org/10.1525/elementa.2021.00062)
886 00062.

887 Randelhoff, A., J. Holding, M. Janout, M. K. Sejr, M. Babin, J.-E. Tremblay, and M. B. Alkire,
888 2020: Pan-Arctic Ocean Primary Production Constrained by Turbulent Nitrate Fluxes. *Frontiers*
889 *in Marine Science*, **7**, <https://doi.org/10.3389/fmars.2020.00150>.

890 Rudels, B., 2015: Arctic Ocean circulation, processes and water masses: A description of ob-
891 servations and ideas with focus on the period prior to the International Polar Year 2007-2009.
892 *Progress in Oceanography*, **132**, 22–67, <https://doi.org/10.1016/j.pocean.2013.11.006>.

893 Rudels, B., E. P. Jones, U. Schauer, and P. Eriksson, 2004: Atlantic sources of the Arc-
894 tic Ocean surface and halocline waters. *Polar Research*, **23 (2)**, 181–208, [https://doi.org/](https://doi.org/10.1111/j.1751-8369.2004.tb00007.x)
895 10.1111/j.1751-8369.2004.tb00007.x.

896 Seland, O., and Coauthors, 2020: The Norwegian Earth System Model, NorESM2 – Evaluation
897 of theCMIP6 DECK and historical simulations. *Geoscientific Model Development Discussions*,
898 **13 (February)**, 1–68, <https://doi.org/10.5194/gmd-2019-378>.

899 Sellar, A. A., and Coauthors, 2020: Implementation of U.K. Earth System Models for CMIP6.
900 *Journal of Advances in Modeling Earth Systems*, **12 (4)**, e2019MS001946, [https://doi.org/](https://doi.org/10.1029/2019MS001946)
901 10.1029/2019MS001946.

902 Serreze, M. C., and Coauthors, 2006: The large-scale freshwater cycle of the Arctic. *Journal of*
903 *Geophysical Research*, **111 (C11)**, <https://doi.org/10.1029/2005JC003424>.

904 Shen, Z., A. Duan, D. Li, and J. Li, 2021: Assessment and Ranking of Climate Models in Arctic
905 Sea Ice Cover Simulation: From CMIP5 to CMIP6. *Journal of Climate*, **34 (9)**, 3609–3627,
906 <https://doi.org/10.1175/JCLI-D-20-0294.1>.

- 907 Shepherd, A., and Coauthors, 2020: Mass balance of the Greenland Ice Sheet from 1992 to 2018.
908 *Nature*, **579 (7798)**, 233–239, [https://doi.org/https://doi.org/10.1038/s41586-019-1855-2](https://doi.org/10.1038/s41586-019-1855-2).
- 909 Shu, Q., Q. Wang, Z. Song, F. Qiao, J. Zhao, M. Chu, and X. Li, 2020: Assessment of sea ice
910 extent in CMIP6 with comparison to observations and CMIP5. *Geophysical Research Letters*,
911 **47 (9)**, e2020GL087965, <https://doi.org/10.1029/2020GL087965>.
- 912 Shu, Q., Q. Wang, J. Su, X. Li, and F. Qiao, 2019: Assessment of the Atlantic water layer in the
913 Arctic Ocean in CMIP5 climate models. *Climate Dynamics*, **53 (9)**, 5279–5291, <https://doi.org/10.1007/s00382-019-04870-6>.
- 914
- 915 Smedsrud, L. H., and Coauthors, 2022: Nordic Seas Heat Loss, Atlantic Inflow, and Arctic Sea Ice
916 Cover Over the Last Century. *Reviews of Geophysics*, **60 (1)**, e2020RG000725, <https://doi.org/10.1029/2020RG000725>.
- 917
- 918 Solomon, A., and Coauthors, 2021: Freshwater in the Arctic Ocean 2010–2019. *Ocean Science*,
919 **17 (4)**, 1081–1102, <https://doi.org/10.5194/os-17-1081-2021>.
- 920 Steele, M., G. L. Mellor, and M. G. Mcphee, 1989: Role of the Molecular Sublayer in the Melting
921 or Freezing of Sea Ice. *Journal of Physical Oceanography*, **19 (1)**, 139–147, [https://doi.org/10.1175/1520-0485\(1989\)019<0139:ROTMSI>2.0.CO;2](https://doi.org/10.1175/1520-0485(1989)019<0139:ROTMSI>2.0.CO;2).
- 922
- 923 Stroeve, J., and D. Notz, 2018: Changing state of Arctic sea ice across all seasons. *Environmental*
924 *Research Letters*, **13 (10)**, 103001, <https://doi.org/10.1088/1748-9326/aade56>.
- 925 Swart, N. C., and Coauthors, 2019: The Canadian Earth System Model version 5
926 (CanESM5.0.3). *Geoscientific Model Development*, **12 (11)**, 4823–4873, <https://doi.org/10.5194/gmd-12-4823-2019>.
- 927
- 928 Tailleux, R., 2009: Understanding mixing efficiency in the oceans: do the nonlinearities of
929 the equation of state for seawater matter? *Ocean Science*, **5 (3)**, 271–283, <https://doi.org/10.5194/os-5-271-2009>.
- 930
- 931 Tatebe, H., and Coauthors, 2019: Description and basic evaluation of simulated mean state, internal
932 variability, and climate sensitivity in MIROC6. *Geoscientific Model Development*, **12 (7)**, 2727–
933 2765, <https://doi.org/10.5194/gmd-12-2727-2019>.

- 934 Timmermans, M. L., and J. Marshall, 2020: Understanding Arctic Ocean Circulation: A Review
935 of Ocean Dynamics in a Changing Climate. *Journal of Geophysical Research: Oceans*, **125** (4),
936 1–70, <https://doi.org/10.1029/2018JC014378>.
- 937 Timokhov, L., and F. Tanis, 1997: Environmental Working Group Joint U.S.-Russian Atlas of the
938 Arctic Ocean, Version 1. <https://doi.org/10.7265/N5H12ZX4>.
- 939 Treshnikov, A. F., 1985: Arctic atlas. *Head Administration of Geodesy and Cartography of the*
940 *Soviet Ministry, Moscow*, 204.
- 941 Tsubouchi, T., K. Våge, B. Hansen, K. M. H. Larsen, S. Østerhus, C. Johnson, S. Jónsson,
942 and H. Valdimarsson, 2021: Increased ocean heat transport into the Nordic Seas and Arctic
943 Ocean over the period 1993–2016. *Nature Climate Change*, **11** (1), 21–26, [https://doi.org/](https://doi.org/10.1038/s41558-020-00941-3)
944 [10.1038/s41558-020-00941-3](https://doi.org/10.1038/s41558-020-00941-3).
- 945 Tsujino, H., and Coauthors, 2020: Evaluation of global ocean–sea-ice model simulations based on
946 the experimental protocols of the Ocean Model Intercomparison Project phase 2 (OMIP-2). *Geo-*
947 *scientific Model Development*, **13** (8), 3643–3708, <https://doi.org/10.5194/gmd-13-4595-2020>.
- 948 Wang, Q., J. Marshall, J. Scott, G. Meneghello, S. Danilov, and T. Jung, 2019: On the Feedback
949 of Ice–Ocean Stress Coupling from Geostrophic Currents in an Anticyclonic Wind Regime
950 over the Beaufort Gyre. *Journal of Physical Oceanography*, **49** (2), 369–383, [https://doi.org/](https://doi.org/10.1175/JPO-D-18-0185.1)
951 [10.1175/JPO-D-18-0185.1](https://doi.org/10.1175/JPO-D-18-0185.1).
- 952 Wang, Q., and Coauthors, 2016: An assessment of the Arctic Ocean in a suite of interannual
953 CORE-II simulations. Part II: Liquid freshwater. *Ocean Modelling*, **99**, 86–109, [https://doi.org/](https://doi.org/10.1016/j.ocemod.2015.12.009)
954 [10.1016/j.ocemod.2015.12.009](https://doi.org/10.1016/j.ocemod.2015.12.009).
- 955 Wang, S., Q. Wang, M. Wang, G. Lohmann, and F. Qiao, 2021: Arctic Ocean liquid freshwater
956 in CMIP6 coupled models. *Earth and Space Science Open Archive ESSOAr*, [https://doi.org/](https://doi.org/10.1002/essoar.10505861.1)
957 [10.1002/essoar.10505861.1](https://doi.org/10.1002/essoar.10505861.1).
- 958 Woodgate, R. a., K. Aagaard, J. H. Swift, K. K. Falkner, and W. M. Smethie, 2005: Pacific ventila-
959 tion of the Arctic Ocean’s lower halocline by upwelling and diapycnal mixing over the continental
960 margin. *Geophysical Research Letters*, **32** (18), <https://doi.org/10.1029/2005GL023999>.

- 961 Woodgate, R. a., T. J. Weingartner, and R. Lindsay, 2012: Observed increases in Bering Strait
962 oceanic fluxes from the Pacific to the Arctic from 2001 to 2011 and their impacts on the
963 Arctic Ocean water column. *Geophysical Research Letters*, **39** (24), [https://doi.org/10.1029/](https://doi.org/10.1029/2012GL054092)
964 2012GL054092.
- 965 Wu, T., and Coauthors, 2019: The Beijing Climate Center Climate System Model (BCC-CSM): the
966 main progress from CMIP5 to CMIP6. *Geoscientific Model Development*, **12** (4), 1573–1600,
967 <https://doi.org/10.5194/gmd-12-1573-2019>.
- 968 Xin-Yao, R., L. I. Jian, C. Hao-Ming, X. I. N. Yu-Fei, S. U. Jing-Zhi, and H. U. A. Li-Juan, 2019:
969 Introduction of CAMS-CSM model and its participation in CMIP6. *Advances in Climate Change*
970 *Research*, **15** (5), 540, <https://doi.org/10.12006/j.issn.1673-1719.2019.186>.
- 971 Yasunaka, S., and Coauthors, 2018: Arctic Ocean CO₂ uptake: an improved multiyear estimate
972 of the air-sea CO₂ flux incorporating chlorophyll a concentrations. *Biogeosciences*, **15** (6),
973 1643–1661, <https://doi.org/10.5194/bg-15-1643-2018>, URL [https://bg.copernicus.org/articles/](https://bg.copernicus.org/articles/15/1643/2018/)
974 15/1643/2018/.
- 975 Yukimoto, S., and Coauthors, 2019: The Meteorological Research Institute Earth System Model
976 Version 2.0, MRI-ESM2.0: Description and Basic Evaluation of the Physical Component.
977 *Journal of the Meteorological Society of Japan. Ser. II*, **97** (5), 931–965, [https://doi.org/10.](https://doi.org/10.2151/jmsj.2019-051)
978 2151/jmsj.2019-051.
- 979 Zanoski, H., A. Jahn, and M. M. Holland, 2021: Arctic Ocean Freshwater in CMIP6 Ensembles:
980 Declining Sea Ice, Increasing Ocean Storage and Export. *Journal of Geophysical Research:*
981 *Oceans*, **126** (4), e2020JC016930, <https://doi.org/10.1029/2020JC016930>.